

# DESIGN OF AN ANTENNA MEASUREMENT SYSTEM

by

Kyle Patel

A thesis submitted to the Faculty and the Board of Trustees of the Colorado School of Mines in partial fulfillment of the requirements for the degree of Master of Science (Electrical Engineering).

Golden, Colorado

Date \_\_\_\_\_

Signed: \_\_\_\_\_

Kyle Patel

Signed: \_\_\_\_\_

Dr. Atef Z. Elsherbeni  
Thesis Advisor

Golden, Colorado

Date \_\_\_\_\_

Signed: \_\_\_\_\_

Dr. Atef Z. Elsherbeni  
Chair Professor and Department Head  
Electrical Engineering Department

## ABSTRACT

Modern communication systems require next generation antenna, whose performance can only be verified through specialized equipment and methodology. For example, a vector network analyzer can be used to determine metrics such as the impedance bandwidth of an antenna. However, a vector network analyzer provides only a portion of the operational characteristics of an antenna. Instead, controlled environments known as anechoic chambers are used to ascertain the radiation characteristics of an antenna under test. These facilities typically incorporate a variety of different instruments to facilitate the measurement process. Rotary tables, linear actuators, vector network analyzers, and amplifiers are examples of typical components that are used in an anechoic chamber. While one could certainly manually control these components, it is more efficient to automate the measurement procedure. This saves time and increases repeatability of measurements.

This thesis presents a complete software design for automated antenna measurement system for use in anechoic chambers. This developed software is both modular and flexible, which allows for easy adaptation for new equipment over time and allows the system to run in a simulation mode if some hardware components are not present. The system has also proven its capability by successfully measuring the radiation pattern of a dipole antenna, even in an anechoic chamber lacking wall-to-wall absorbers.

## TABLE OF CONTENTS

ABSTRACT .....	iii
LIST OF FIGURES .....	vi
ACKNOWLEDGEMENTS .....	ix
CHAPTER 1 INTRODUCTION TO ANTENNA RADIATION MEASUREMENT SYSTEMS .....	1
1.1 Overview of Antenna Radiation Characterization Methods .....	1
1.2 Automated Measurement Benefits .....	6
1.3 Previous Work in Automated Far-Field Measurement .....	7
1.4 Proposed Automated Measurement Design .....	8
CHAPTER 2 AUTOMATED MEASUREMENT SYSTEM OVERVIEW AND USAGE ....	10
2.1 Rotators .....	10
2.2 Linear Actuators .....	11
2.3 Vector Network Analyzer .....	11
2.4 Low-Noise Amplifier .....	12
2.5 General Operating Procedure .....	12
CHAPTER 3 SOFTWARE DESIGN AND USAGE .....	15
3.1 Design .....	15
3.2 Usage .....	20
CHAPTER 4 DIPOLE MEASUREMENT EXAMPLE .....	29
CHAPTER 5 FUTURE UPGRADES AND CONCLUSION .....	40
REFERENCES .....	43

APPENDIX A DATA PARSER CODE..... 45

## LIST OF FIGURES

Figure 1.1	The three field regions for an antenna, where D is the largest dimension of the antenna under test.....	2
Figure 1.2	E and H-field probes used in near-field measurements.....	2
Figure 1.3	The proposed automated antenna measurement system.....	5
Figure 1.4	Previous antenna measurement system design using MATLAB [14].....	7
Figure 2.1	One of the Velmex B4872TS rotary tables (left) and one of the VXM Stepping Motor Controllers (right).....	10
Figure 2.2	The y-axis linear actuator (bottom-left) housed in the source fixture.....	11
Figure 2.3	The Keysight E5080A ENA (left) and the Keysight FieldFox N9918A (right).....	12
Figure 2.4	The ZVA-183-S+ amplifier connected to the system.....	13
Figure 2.5	The general software procedure for taking a measurement.....	13
Figure 3.1	Diagram of code class names and their dependencies for the automated measurement system software.....	15
Figure 3.2	UML diagram for the Rotator class.....	17
Figure 3.3	UML diagram for the YZ Translator class.....	17
Figure 3.4	UML diagram for the Measurement Engine class.....	19
Figure 3.5	UML diagram for the Plotter class.....	19
Figure 3.6	Flowchart of software measurement procedure.....	21
Figure 3.7	The ‘Aenchoic Init’ window.....	21
Figure 3.8	Automated measurement system software main GUI.....	22
Figure 3.9	The ‘Rotator Setup’ section of the software interface.....	23
Figure 3.10	The linear actuator setup section of the software interface.....	24
Figure 3.11	The ‘Measurement Setup’ section of the software interface.....	24
Figure 3.12	The ‘Plot Display Options’ section of the software interface.....	25

Figure 3.13	The ‘System Messages’ section of the software interface.....	26
Figure 3.14	The plot window where $S_{21}$ data is plotted during a measurement.....	26
Figure 3.15	Truncated example of the data file automatically saved by the measurement system.....	27
Figure 3.16	Rectangular plot of the data slice returned by the ‘DataParser’ method from a file containing data for a y-z plane-cut of a dipole.....	28
Figure 4.1	The 2.4 GHZ dipole antenna mounted onto the AUT fixture.....	29
Figure 4.2	The E5080A VNA used for the measurement example.....	30
Figure 4.3	The startup configuration needed for the measurement example.....	30
Figure 4.4	Initializing the rotators for the measurement example.....	31
Figure 4.5	Initializing the linear actuators for the measurement example.....	31
Figure 4.6	Aligning the source fixture for the AUT via the interface.....	32
Figure 4.7	Source fixture before alignment (left) and source fixture after alignment (right).....	32
Figure 4.8	Setting up the measurement parameters for the y-z plane-cut of the measurement example.....	33
Figure 4.9	Adjusting the polar parameters for the measurement example.....	34
Figure 4.10	In-progress plotting of the y-z plane-cut for the measurement example.....	34
Figure 4.11	In-progress measurement of the y-z plane-cut for the measurement example.....	35
Figure 4.12	The final plot of the y-z plane-cut data for the measurement example.....	35
Figure 4.13	Setting up the measurement parameters for the x-y plane-cut of the measurement example.....	36
Figure 4.14	Source antenna moved to the vertical position for the x-y plane-cut of the measurement example.....	36
Figure 4.15	Offsetting the R1 rotor for the x-y plane-cut of the measurement example.....	37

Figure 4.16	The R1 rotor offset for the x-y plane-cut of the measurement example.....	38
Figure 4.17	In-progress plotting of the x-y plane-cut data for the measurement example.....	38
Figure 4.18	In-progress measurement of the x-y plane-cut for the measurement example.....	39
Figure 4.19	The final plot of the x-y plane-cut data for the measurement example.....	39

## ACKNOWLEDGEMENTS

I would like to thank Robert Jones for his work on designing and constructing the crucial mechanical structures and mounts this automated antenna measurement system depends on. This work would also not be possible without the help and guidance of my thesis advisor Dr. Atef Elsherbeni, who spent many early mornings reviewing my work and last-minute drafts. I would also like to thank Dr. Chris Coulston and Dr. Payam Nayeri for being a part of my committee and making room in their busy schedules for the defense. Lastly, I would also like to thank the Colorado School of Mines Electrical Engineering Department for supporting my graduate study.

## CHAPTER 1

### INTRODUCTION TO ANTENNA RADIATION MEASUREMENT SYSTEMS

Antennas are vital in an ever-connected modern society. The need for higher performing antennas increases with the need for more robust wireless devices. Thus, it is important for engineers to have tools to better quantify the performance of fabricated antennas. One can easily get metrics such as the impedance bandwidth of an antenna from standard microwave equipment such as a vector network analyzer (VNA) [1]. However, this is only a small slice of the overall performance of an antenna. Some of the more vital characteristics of any antenna are its radiation qualities. Characteristics such as gain, radiation pattern, and axial ratio require specialized tools, methods, and facilities to determine experimentally [2-3].

#### **1.1 Overview of Antenna Radiation Characterization Methods**

Radiation qualities of an antenna can be determined from two types of measurements: near-field measurement [4] and far-field measurement [5]. These correspond to different antenna radiation regions, where electromagnetic fields behave differently [2]. The three regions, reactive near-field, radiating near-field, and far-field, and their criteria are shown in Figure 1.1. Measurements are typically performed in the first and third regions.

##### **1.1.1 Near-Field Measurements of Antenna Radiation**

The reactive near-field of an antenna is dominated by reactive fields, which results in little real propagated power transferred to a receiver. Most power transfer will occur through coupling mechanisms that occur at very small distances. To characterize the radiation qualities of an antenna in this region, one typically uses E or H-field probes attached to a spectrum analyzer or similar microwave device [6]. Examples of these probes are shown in Figure 1.2. The E-field probe

consists of a center conductor extending out of a larger outer shield. This forms a coaxial dipole, which can be used to detect changing electric fields. The magnetic field probe consists of a loop of shielded wire that forms a closed circuit. Its operation can be explained by Faraday's law [7-8].

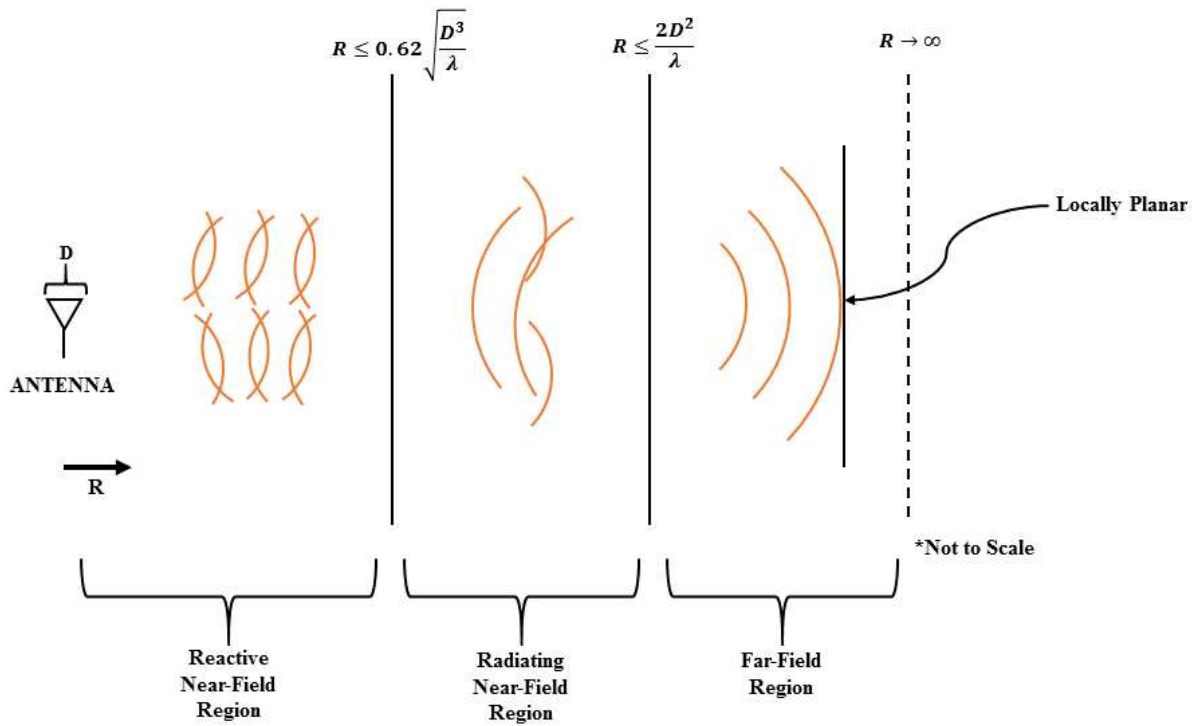


Figure 1.1 The three field regions for an antenna, where  $D$  is the largest dimension of the antenna under test.

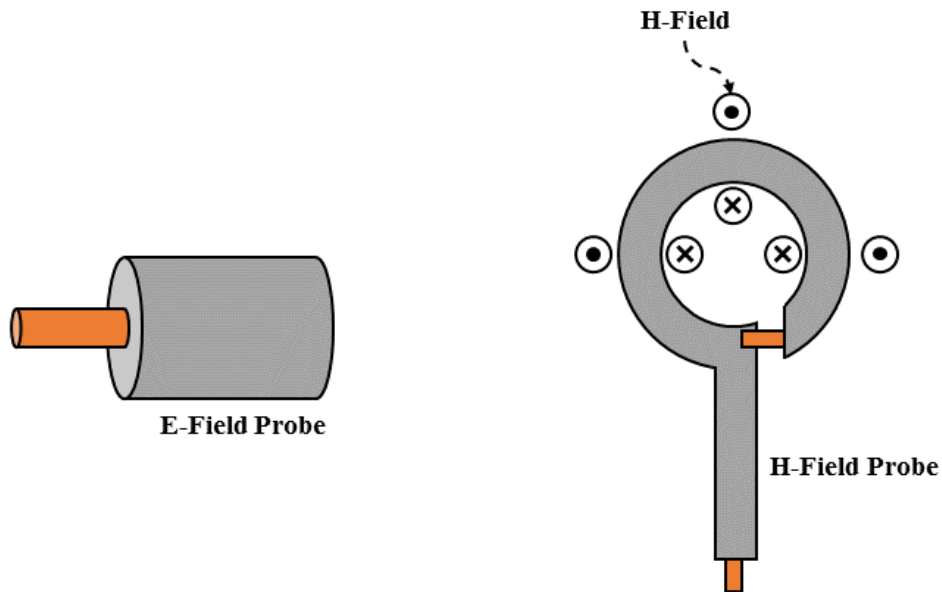


Figure 1.2 E and H-field probes used in near-field measurements.

There are three main methods of utilizing these field probes to characterize an antenna: planar measurement, cylindrical measurement, and spherical measurement. These different methods refer to the way the probe is swept along the antenna. For instance, the planar measurement involves sweeping a probe in a linear (x, y, or z) direction, whereas the spherical measurement involves sweeping either the probe or antenna through a combination of elevation and azimuth angles at a constant radius [9]. Regardless of the measurement method, there must be some conversion from the near-field data into the far-field data that one is typically interested in. Typically, this is done with various Fourier transform methods [10-11].

Commercially, there exist some comprehensive systems that perform these functions. For instance, the company EMSCAN produces test-beds that incorporate many magnetic field probes in a grid array. These probes can sense the near-field magnetic field of a nearby antenna and determine what the surface currents on the antenna are. From this, the EMSCAN-provided software can apply various transforms to determine the far-field radiation pattern and axial ratio.

### **1.1.2 Far-Field Measurements of Antenna Radiation**

The far-field region of antenna is dominated by fields with no dependence on radial distance. Furthermore, the far-field criteria for an antenna is established such that the fields can form into plane waves, which allows for very little phase and amplitude taper across the aperture of a receiving antenna [2]. For measurements in this region, a source antenna that is known and characterized is used to illuminate the antenna under test (AUT), or antenna with unknown characteristics. The two antennas are usually connected to a vector network analyzer or similar microwave device, where the relative received power from the AUT can be captured and recorded as  $S_{21}$ . The captured data can then be directly used to determine the radiation pattern and can also indirectly determine the characteristics of the AUT. Usually, there must be motors, in the form of

rotary tables, that allow one to rotate one or both antennas to get the full radiation pattern of the AUT as functions of angle and frequency.

Far-field measurements are usually held within far-field ranges, which can be indoor or outdoor. There are two main types of far-field ranges: reflection and free-space. Reflection far-field ranges attempt to get the direct signal from the source antenna to combine constructively with the ground-reflected signal at the AUT. Free-space ranges, by contrast, try to remove the presence of ground-reflected signals entirely. Free-space ranges can also be broken down into three subtypes: elevated range, slant range, and compact range. A common property of all these ranges, except for the compact range, is that the distance between the source and AUT is large enough to meet the far-field criteria of the frequency of interest [12].

The elevated range places each antenna on a tower far above the ground, typically at a height greater than four times the largest dimension of the AUT. This is done so only the sidelobe of the source antenna presents a signal reflected by the ground, which would be negligible compared to the direct path signal. Typically, such ranges are outdoor and require a smooth terrain between the towers. Because these ranges are outdoors and have plenty of space, they are optimal for testing very large diameter antennas [12].

Slant ranges are very similar to elevated ranges. The only difference is that the source antenna is placed directly on the ground and is pointed up at the AUT which is still on a tower. The first null of the source antenna will intercept the tower of the AUT, which is usually covered in a non-conductive material so that the signal will not reflect further. The benefit to the slant range is that it reduces the distance between the two antennas which can be very valuable [12].

The final compact range is a special range that uses a parabolic reflector to transform a spherical wave-front into a planar wave-front in distances that are far shorter than the far-field

distance. This allows for a range that can fit inside a room covered in electromagnetic wave absorbing material, or an anechoic chamber. However, the design and positioning of such a reflector is not a simple task and is often dependent on the AUT [12].

Technically, the anechoic chamber by itself is also a type of indoor free-space range, regardless if a parabolic reflector is used. Because of the property of the electromagnetic wave absorbers lining the walls of the chamber, there are very little reflections within the chamber [12]. This means that one can place two antennas at the ends of the room without worrying about problems that are typical with outdoor ranges, such as the height of the antennas in the elevated range. An example of a typical anechoic chamber measurement setup is shown in Figure 1.3.

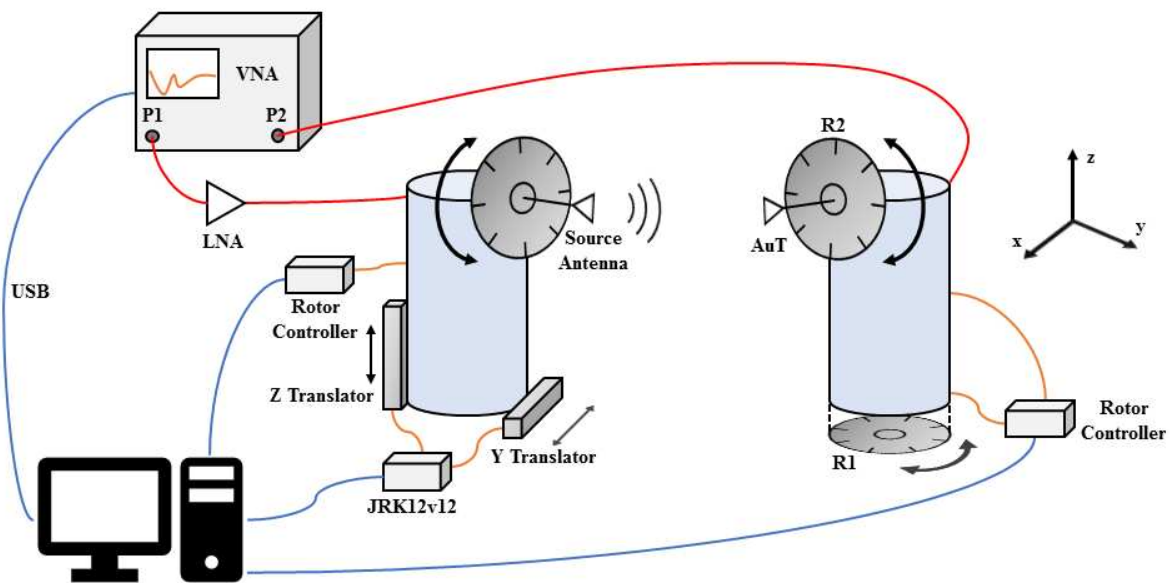


Figure 1.3 The proposed automated antenna measurement system. Red lines indicate radiofrequency cables, orange lines indicate peripheral hardware connections, and blue lines indicate USB connections.

### 1.1.3 Comparison of Near-Field versus Far-Field Measurements

Both near-field and far-field measurement types allow a test engineer to determine the radiation qualities of an antenna. However, there are reasons why one may choose one over the other.

The near-field measurement requires very fine positioning of the probe or antenna. Typically, the distance between measurement points for a planar measurement is less than half wavelength. For high frequencies, this can necessitate very fine, and thereby expensive, positioning schemes. Problems often occur with the mutual coupling of the probe and the antenna, which necessitates further shielding or absorbing materials [13]. However, near-field ranges are much more compact than their far-field equivalents, as the distance between the AUT and the probes is very small. This makes near-field ranges very attractive for antennas at high frequency if space is at a premium. However, near-field ranges tend to perform poorly with low frequency antennas, as they require more sensitive probes.

Far-field measurements are very dependent on the ability to control reflections. For outdoor ranges, this usually requires very smooth terrain and large distances, both of which can be expensive and hard to obtain. Furthermore, there can be many sources of interference when performing a test outdoors. While indoor ranges can be better controlled and protected from external interference, they still require expensive radiofrequency absorbers to reduce reflections within the room. The exorbitant cost of these absorbers can often be a limiting factor to the design of such ranges. Furthermore, the accuracy of the far-field ranges is limited by the finiteness of their size. For large high frequency antennas, the far-field distance would be very large, which would require a very large and expensive range [12].

## **1.2 Automated Measurement Benefits**

In both measurement types, it is beneficial to have an automated electronic positioning and control system that performs the measurement. This brings repeatability, accuracy, and shorter measurement times compared to a manual equivalent. Furthermore, this allows for real-time visualization and analysis of the associated radiation characteristics the test engineer is interested

in. Many of these systems incorporate many different motors and microwave measurement devices, which makes it even more beneficial to be able to control everything from a unified graphical user interface (GUI).

### 1.3 Previous Work in Automated Far-Field Measurement

There have been previous attempts at creating an automated measurement system (AMS) for use within anechoic chambers. One such example was done at the University of Mississippi by Garner [14]. The result of his work is shown in Figure 1.4. The physical configuration of the system was similar to that of Figure 1.3, but with only the source antenna rotor, the R2 rotor, and the VNA.

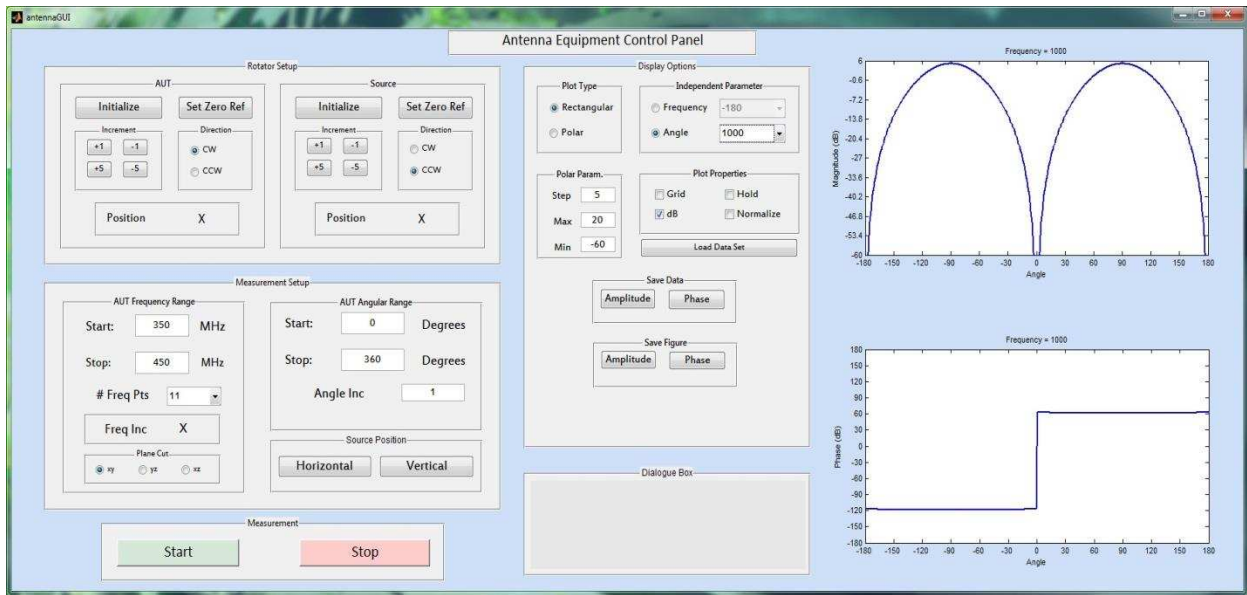


Figure 1.4 Previous antenna measurement system design using MATLAB [14].

The result of that work allowed for a test engineer to control the entirety of a basic  $S_{21}$  measurement with a VNA as a function of frequency and angle from the MATLAB based interface. The user could then plot the magnitude and phase of  $S_{21}$  on the computer.

This work showed great promise as it could give the user a radiation pattern by controlling the VNA and the individual antenna rotors from Velmex. However, there were some limitations typically associated with this first-prototype software. While an object-oriented model was followed, there was not a proper separation of hardware peripheral logic and GUI code, which meant that the software could not be easily changed without digging through many lines of inter-related code. This also meant that the software would not function without significant overhaul should one of the underlying components have to be replaced or upgraded (such as different rotary tables). Furthermore, the MATLAB code relied heavily on toolboxes in order to perform the VNA communication. This is inconvenient from a deployment perspective as it adds additional dependencies that could change over time or add cost. The software was also coded for a very specific VNA, which was fine for the project then, but would not be as ideal in a general deployment scheme. The user experience for the interface could also have been improved in several areas to provide a more clean, procedural, and error-resistant experience. Lastly, the system could not perform any sort of axial ratio measurement, as it lacked a second rotor on the AUT side to enable this functionality.

#### **1.4 Proposed Automated Measurement Design**

The proposed antenna measurement system is written as a modern replacement for previous designs [14-15]. It follows modern programming design principles and implementation. Specifically, the design separates the peripheral hardware logic (PHL) from the GUI, and abstracts each PHL unit into independent classes that can be replaced or updated as needed. This allows for the same base system to be used indefinitely, while still maintaining the same operator experience through revisions. The user interface itself has also been reworked to be more procedural and lessen the chance the operator can break the system.

Not only are there maintainability and deployment improvements to the software, but there are additional capabilities proposed. The new design allows for axial ratio measurements due to the inclusion of a second rotary table on the AUT side. It also includes two linear actuators that can be used to translate the source antenna in the y and z directions for better alignment with the AUT. Finally, it also includes unique capability to work with any modern virtual instrument software architecture (VISA)-compatible Keysight VNA through a simple USB or ethernet interface. This is preferable to the old GPIB (IEEE-488) based approach for two main reasons: GPIB is a dated interface that fewer people in the future will understand, and because GPIB is dated, it often requires expensive adapters to connect to regular consumer computers. Modern USB and ethernet connections are cheap, abundant, better understood, and best of all, faster. A system diagram of the proposed system can be reviewed in Figure 1.3.

## CHAPTER 2

### AUTOMATED MEASUREMENT SYSTEM OVERVIEW

This section outlines the different hardware components that the system utilizes to characterize the antenna under test. The software is expected to be able to interface and function with these components.

#### 2.1 Rotators

Rotators are used to precisely orient antennas used in the measurement process. For this anechoic chamber, three Velmex B4872TS rotary tables are used as the rotator elements [16]. These units utilize precision stepper motors that allow for full 360-degree rotation with 0.0125-degree repeatable accuracy. Two of these units are used in the antenna under test side of the chamber, while one is used for the source transmitter antenna. The rotary tables connect to Velmex VXM Stepping Motor Controllers which then communicate to a computer via a RS232 interface. These controllers allow for complete software control of the speed, direction, and position of the individual rotators. These controllers also allow the software to query the state of each individual rotator. Figure 2.1 shows a rotary table and controller in use.



Figure 2.1 One of the Velmex B4872TS rotary tables (left) and one of the VXM Stepping Motor Controllers (right).

## 2.2 Linear Actuators

Two Pololu LACTP linear actuators are used in the transmitter side for precise alignment with the AUT in the y and z-axes of the transmitter frame of reference [17]. This allows the center of the source antenna to be better aligned with the center of the antenna under test. These actuators are controlled via the Pololu JRK12v12 Controller which can be commanded via an RS232 interface. The y-axis actuator has 101.6 mm of drive length and the z-axis actuator has 152.4 mm of drive length. They can be positioned to an accuracy of 0.1 mm. Figure 2.2 shows the z-axis actuator used.

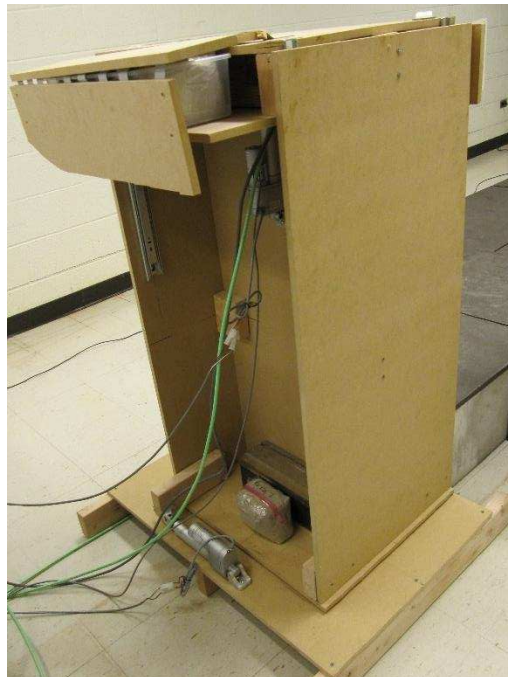


Figure 2.2 The y-axis linear actuator (bottom-left) housed in the source fixture.

## 2.3 Vector Network Analyzer

Two different VNAs are used to perform high frequency measurements of the antenna under test. The Keysight E5080A ENA, connected by USB to the main computer, allows for measurements between 100 KHz and 9 GHz. Alternatively, the Keysight Fieldfox N9918A VNA

can be used for measurements up to 26.5 GHz. The Fieldfox requires an ethernet based connection to the main computer for commanding. The developed software is expected to be able to utilize either type of VNA seamlessly for use in the antenna under test measurement. The VNAs in use are shown in Figure 2.3.



Figure 2.3 The Keysight E5080A ENA (left) and the Keysight FieldFox N9918A VNA (right).

## 2.4 Low-Noise Amplifier

A ZVA-183-S+ Super Ultra Wideband Amplifier from Mini-Circuits is used to compensate for system losses at high frequencies. The amplifier works from 700 MHz to 18 GHz and features a typical gain of 26 dB and noise figure of 3 dB. It requires a power supply capable of providing 12 V and 500 mA to be biased on. The input of the amplifier is connected to the VNA port one and the amplifier output is connected to the source transmitting antenna. Figure 2.4 depicts the amplifier connected to the system.

## 2.5 General Operating Procedure

In preparation for a measurement, the user should first follow a general hardware startup procedure:

1. Turn on the two VXM Stepping Motor Controllers through the power switch housed on the controllers themselves.
2. Plug the power supply for the linear actuators into a wall outlet.
3. Select a VNA and ensure it is ready for communication.
  - a. For the E5080A ENA, the user should login and open the VNA desktop application.
  - b. For the FieldFox N9918A, the user should turn on the VNA and apply the NA mode setting.

Once this setup is performed, the user may then start the software through MATLAB and follow the general procedure outlined in Figure 2.5.

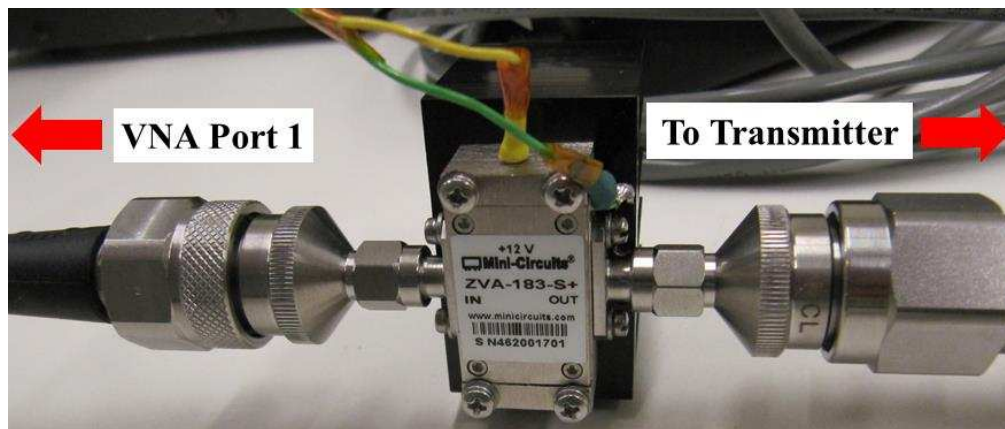


Figure 2.4 The ZVA-183-S+ amplifier connected to the system.



Figure 2.5 The general software procedure for taking a measurement.

Using the software, one would setup and initialize the rotary tables and then the linear actuators. Next, the user would define the plane sweep and angles of rotation for the rotators. The

user would then specify the VNA settings such as frequency range, number of frequency points, and output power level. At this time, the user may also change the default plot display options so that they are viewing the data they are interested in. Finally, the user can start the automated measurement process. Before doing so, the user should turn on the power supply for the amplifier through the switch on the power supply frame. Once the measurement is complete, the user should turn off the amplifier power supply. The data is automatically saved as a csv file. Once the user is done taking measurements, the software interface should be closed and then the hardware components should be turned off in the reverse order of the hardware startup procedure:

1. Turn off the VNA.
2. Unplug the power supply for the linear actuators from the wall outlet.
3. Turn off the two VXM Stepping Motor Controllers through the power switch housed on the controllers themselves.

## CHAPTER 3

### SOFTWARE DESIGN

The automated antenna measurement system consists of carefully designed software in MATLAB and C#. The interactions and behavior of this software is explained in this chapter.

#### 3.1 Design

The automated measurement system is broken into several code units and classes. These code classes can be reviewed in Figure 3.1 and are explained in detail in the following sections.

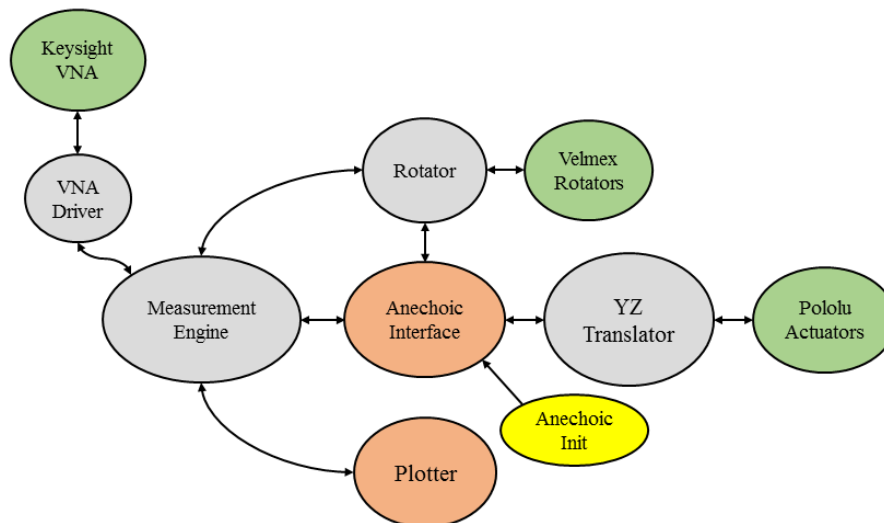


Figure 3.1 Diagram of code class names and their dependencies for the automated measurement system software. The grey entities are names of code objects, the green entities are the names of hardware components, and the orange entities are GUI names. The yellow entity is name for the code that serves as the entry point for the software.

##### 3.1.1 Anechoic Init

This code unit consists of an interface that serves as the entry point for the entire program. This allows the user to select whether different components are simulated as well as the specific VNA the user wishes to use in the measurement. Anechoic Init then starts the main Anechoic Interface code unit with these parameters.

### **3.1.2 Anechoic Interface**

This code unit is responsible for handling all GUI related tasks. This provides the user with an interactive and dynamic display that allows full control over the antenna measurement process. Anechoic Interface calls upon the API of the other peripheral code units to command, control, and monitor actual hardware elements of the antenna measurement system. This code unit only contains logic for displaying and taking inputs from the user, which allows the GUI to be changed independently of the underlying control logic for the different hardware peripherals.

### **3.1.3 Rotator**

The Rotator class exposes API that allows for complete interaction with the Velmex rotary tables. It can command each rotary table to a specific angle, either through an absolute or a relative positioning scheme. It also keeps track of the current position of each rotor in real time and can calculate the true position of any rotor even with user applied offsets. The Rotator class can be invoked by itself, independent of the other code units, and can be used to test the individual rotary control implementation. The Rotator class is also capable of being invoked in simulation mode, which simulates each rotator but still exposes the same API and behavior the same to external callers. The exposed API can be reviewed in Figure 3.2.

### **3.1.4 YZ Translator**

The YZ Translator class exposes API that allows for complete interaction with the Pololu linear actuators. It can command each linear actuator to a specific linear position, either through an absolute or a relative positioning scheme. The class can also keep track of the actual position of the linear actuators in real time. This class can also be invoked independently of the rest of the code units and features a simulation mode identical to the Rotator class. The exposed API can be reviewed in Figure 3.3.

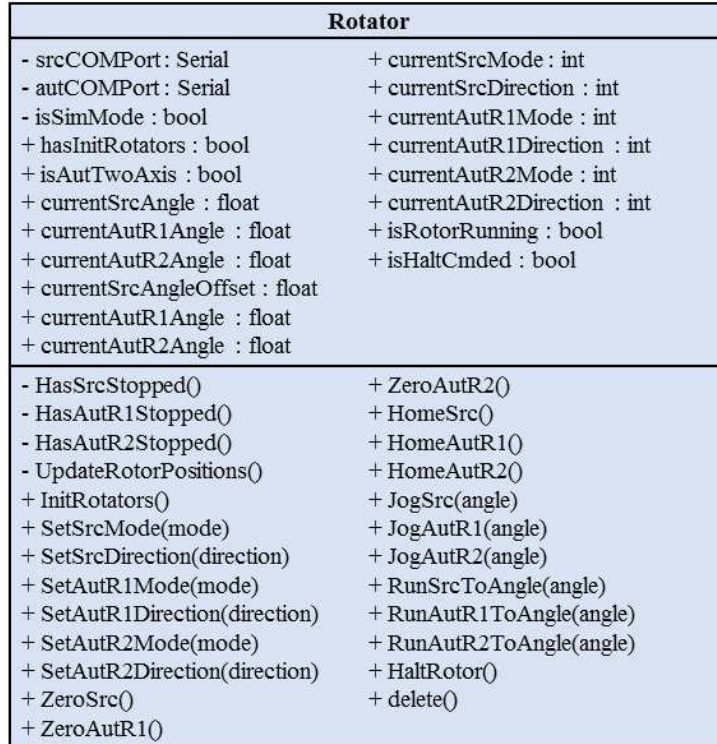


Figure 3.2 UML diagram for the Rotator class.

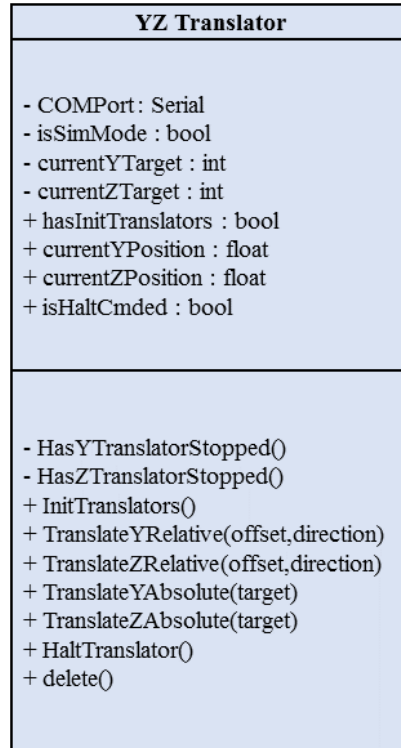


Figure 3.3 UML diagram for the YZ Translator class.

### **3.1.5 Measurement Engine**

The Measurement Engine class exposes API that allows for complete control over the measurement setup for a given measurement scenario. It is dependent on the Rotator, VNA Driver, and Plotter classes to function. This class takes in various user inputs from Anechoic Interface that define the measurement the user wants. Examples of such parameters are VNA start/stop frequency, VNA output power level, and angles of rotation for each rotor. The Measurement Engine then utilizes the Rotator class to move each motor to the requested sweep angles. At each angle, the class then invokes the VNA Driver to get  $S_{21}$  for the entire frequency range the user requested. The Measurement Engine then takes this data and saves it in real time to a csv file. At the same time, the class utilizes the Plotter class to display the data that the user requested in the Anechoic Interface. The Measurement Engine also can be invoked with a simulation mode, where the VNA connection is simulated and the VNA Driver class is not invoked. The exposed API can be reviewed in Figure 3.4.

### **3.1.6 Plotter**

The Plotter class exposes API for displaying live data that the user is interested in during and after the measurement process. It can be invoked independently of other classes and can be used to plot data parsed from the csv files output by the system. The class exposes API that allows one to utilize up to two rectangular or two polar plots and plot interpolated data of interest. The user can also control basic plot parameters such as the range and increment between minor values. The exposed API can be reviewed in Figure 3.5.

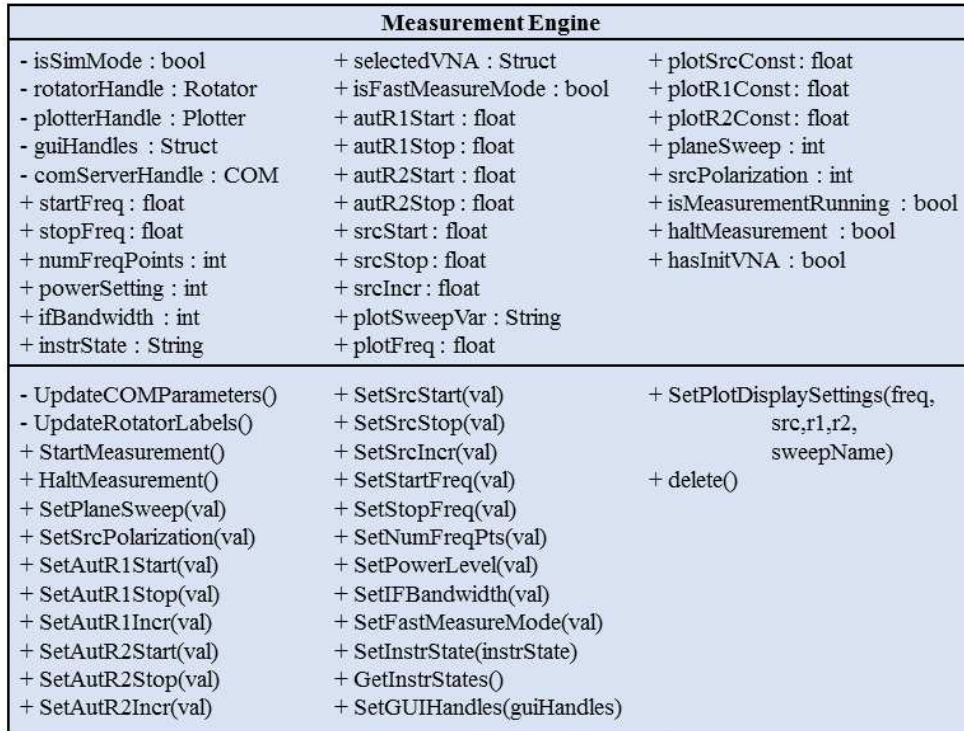


Figure 3.4 UML diagram for the Measurement Engine class.

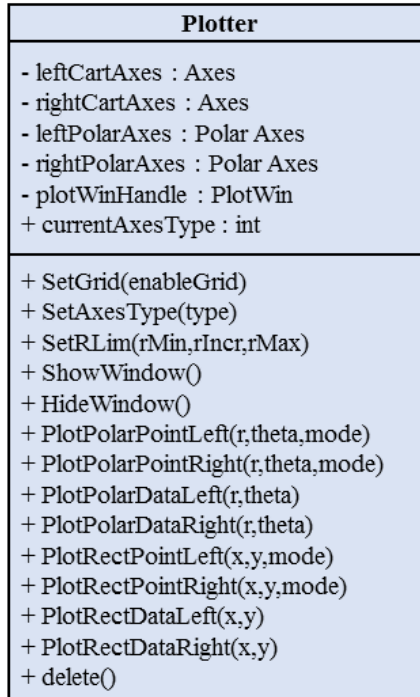


Figure 3.5 UML diagram for the Plotter class.

### **3.1.7 VNA Driver**

The VNA Driver is a C# based code unit that exposes the capability to command and control Keysight VISA compatible VNAs. It communicates to MATLAB via the Windows Common Object Model (COM) framework, which facilitates inter-process communication. Utilizing the COM framework, the driver can directly pull parameters from the MATLAB workspace and then place VNA data directly into the MATLAB workspace. This keeps everything in memory and is much faster than passing parameters and data via the file system.

## **3.2 Usage**

The software interface is designed to give a guided user-experience that is easy to follow in a consistent manner. The flow of sections is arranged in a left-to-right manner, giving a procedural experience that is akin to reading a book. The steps in order are detailed in the following sections. This simple procedure can also be reviewed in Figure 3.6. First, the user starts with the initialization window that allows them to select whether certain components are simulated or not. This also allows the user to select the VNA they are interested in using. This interface is shown in Figure 3.7. Alternatively, the user may also start the main interface directly without the initialization window which will by default run everything in simulation mode. The main interface is shown in Figure 3.8.

### **3.2.1 Rotator Setup**

First, the user will click on one of two initialization buttons depending on the type of measurement the user wants. If the user needs to perform a measurement only in the x-y plane of the AUT side, then the user should select the left button. If the user needs a combination of an x-y plane and y-z plane measurement of the AUT, then the user should select the right button. The

only difference between the two initialization states is that it determines whether the R2 rotor is used.

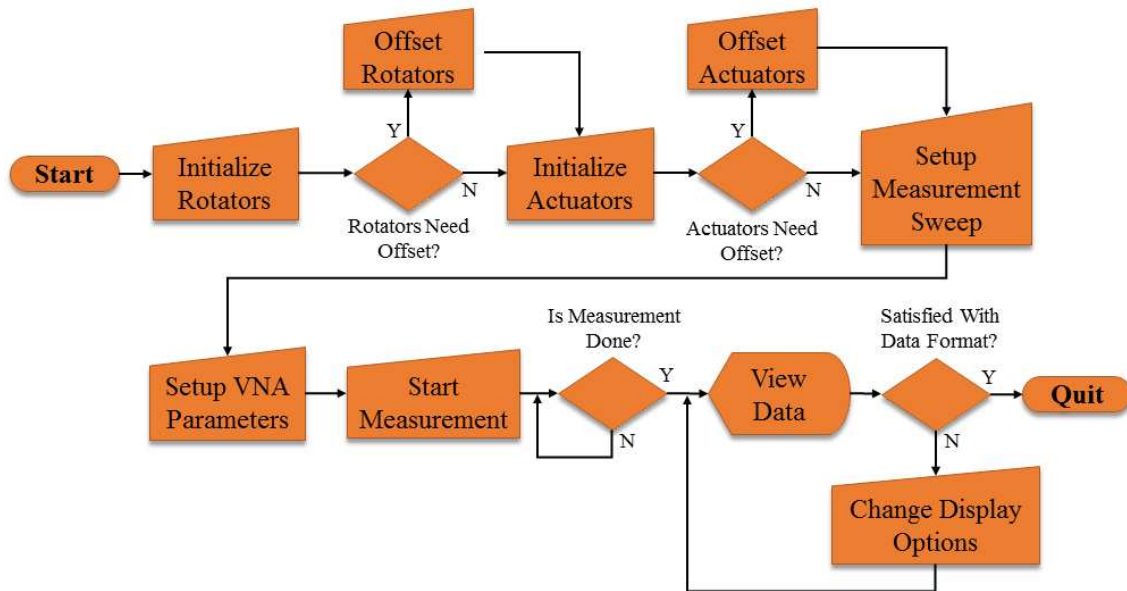


Figure 3.6 Flowchart of software measurement procedure.

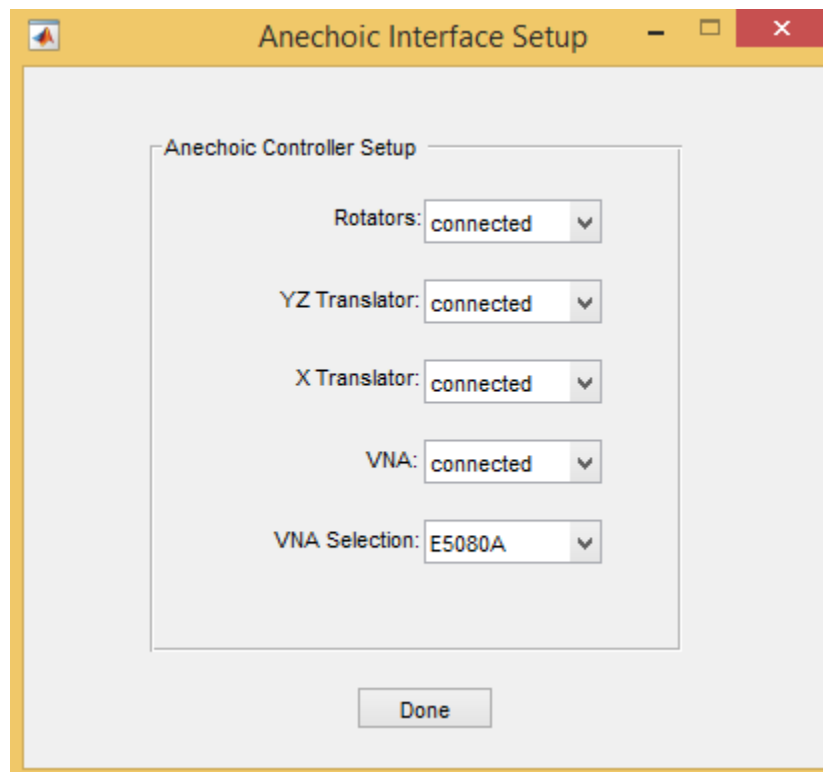


Figure 3.7 The 'Anechoic Init' window.

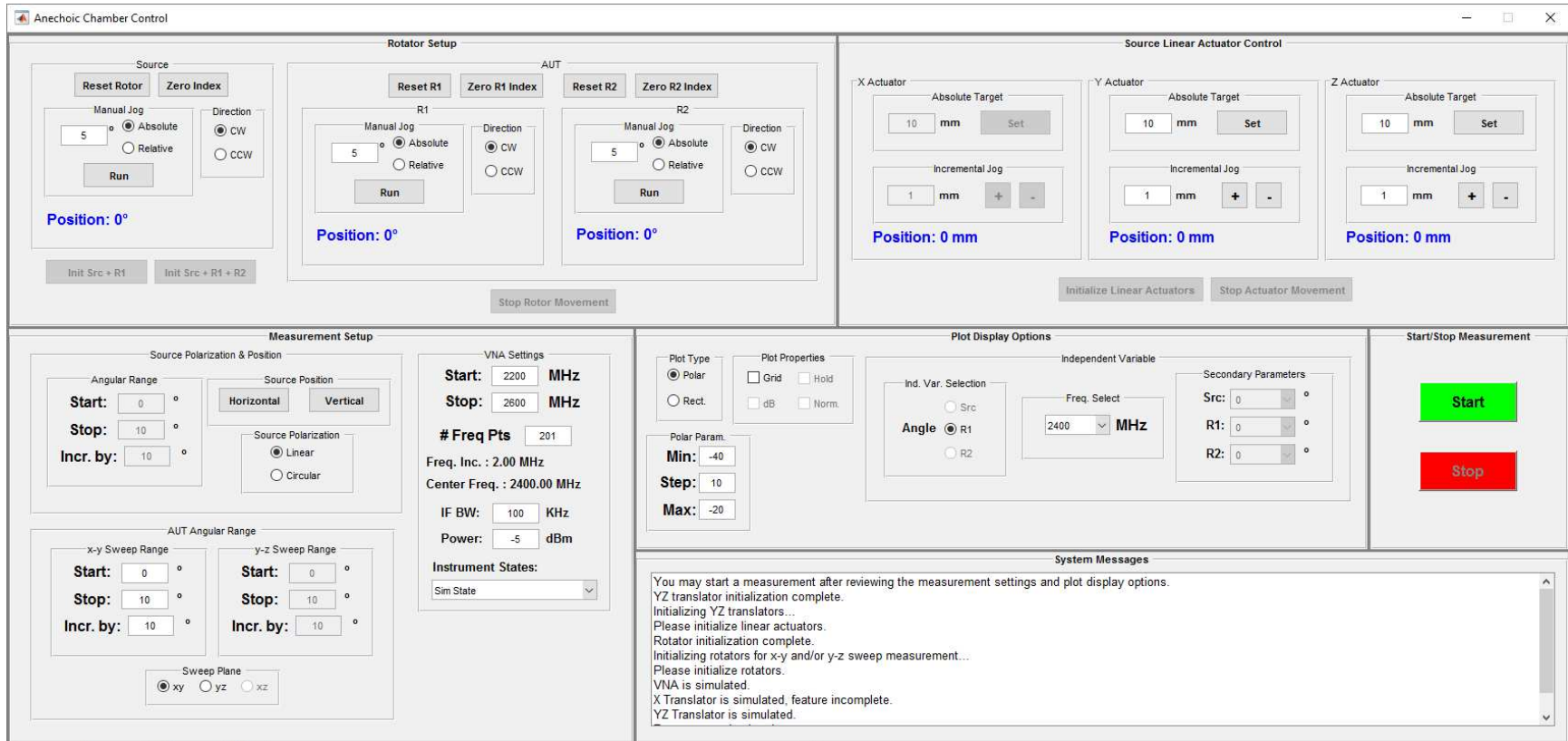


Figure 3.8 Automated measurement system software main GUI.

After the user selects the initialization type for the rotors, a brief homing sequence will run to put the system in a known state. Once this is done, the user may then offset any of the rotors to setup up the proper measurement. The user has full control of each rotor and whether it indexes clockwise, counterclockwise, or in absolute or relative mode. The user can also re-home and zero each rotor. The rotator setup section is shown in detail in Figure 3.9.

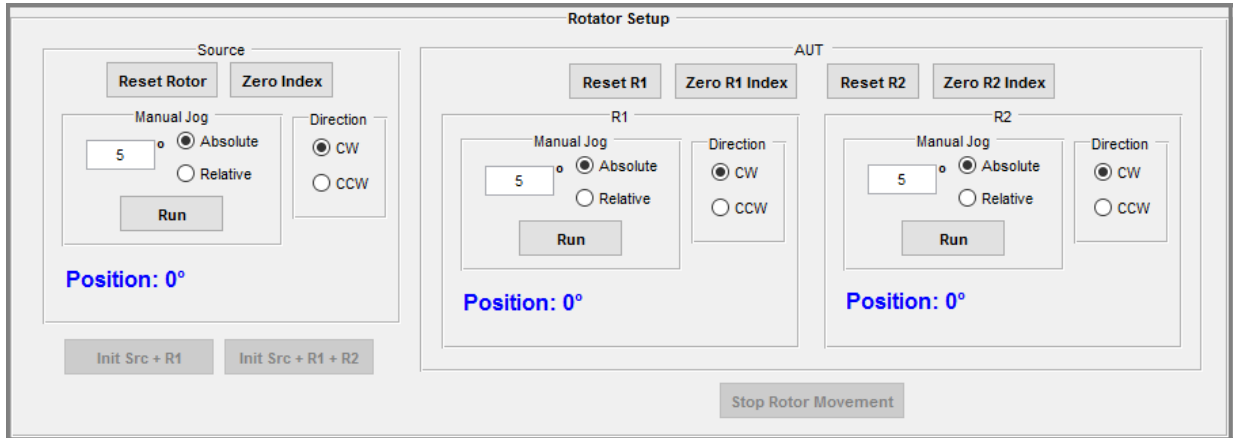


Figure 3.9 The ‘Rotator Setup’ section of the software interface.

### 3.2.2 Source Linear Actuator Control

Next, the user will be asked to initialize the linear actuator system. This will home each actuator and put them in a known position. The user can then position each actuator until the alignment between the transmitter antenna and the AUT is acceptable. The user can either command each translator by absolute or relative positioning. The linear actuator control section is shown in detail in Figure 3.10.

### 3.2.3 Measurement Setup

Here, the user can setup the VNA and measurement parameters. Parameters such as the frequency range, power level, and the IF bandwidth of the VNA can be set here. The rotor to perform the sweep over as well as the sweep parameters are defined here as well. The user may

also provision for a multi-axis sweep by selecting the circular polarization type measurement. The plane-cuts are referenced to the axis of the AUT fixture, which are shown in Figure 1.3.

Once the user is satisfied with the selections, the user can start the measurements by clicking on the green ‘Start’ button. If the user wants to stop the measurement at any time, the user may click the red ‘Stop’ button. The measurement setup section is shown in detail in Figure 3.11.

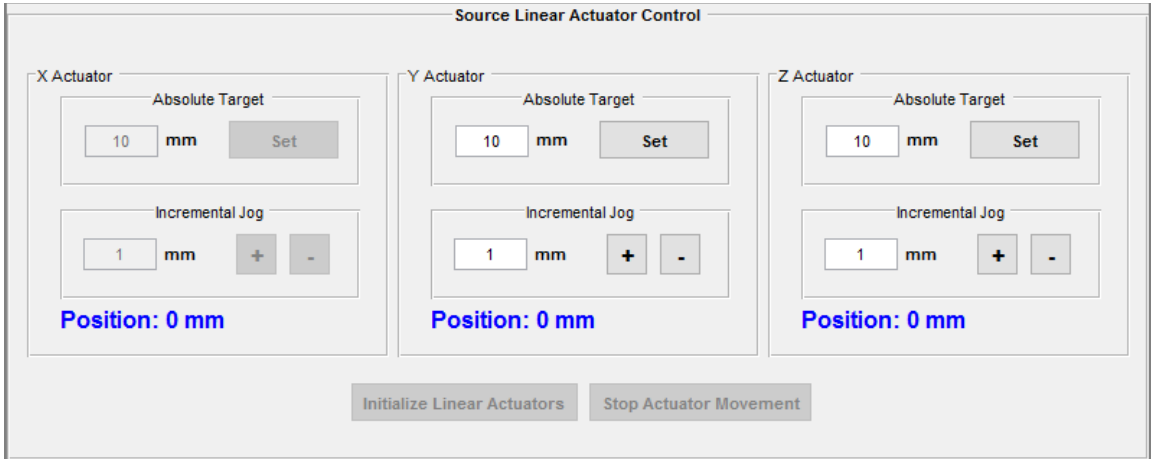


Figure 3.10 The linear actuator setup section of the software interface.

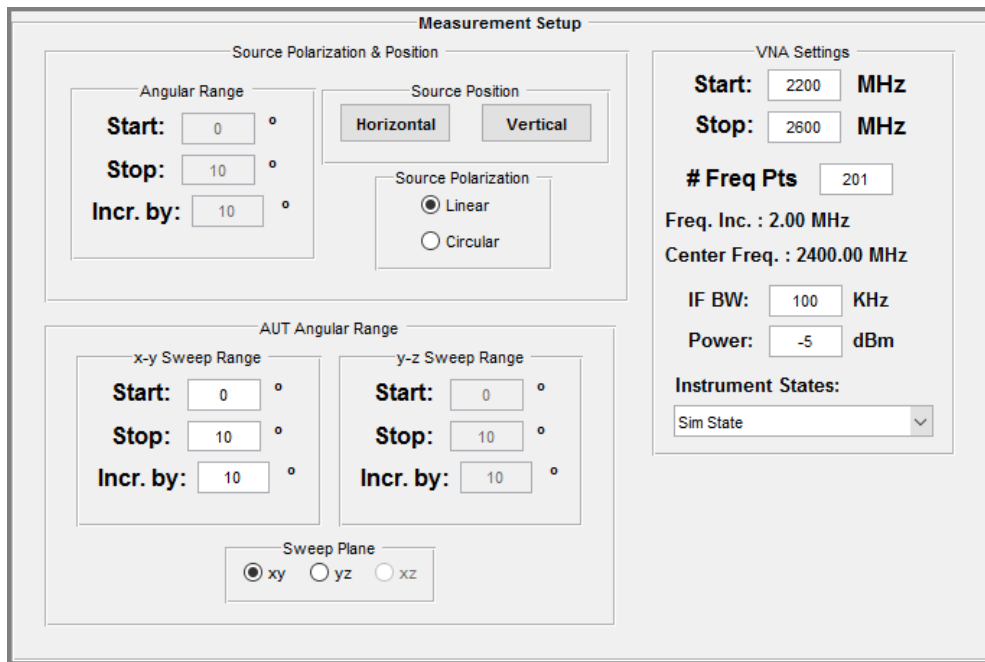


Figure 3.11 The ‘Measurement Setup’ section of the software interface.

### 3.2.4 Display Options

Once the measurement has started, a plot window will appear and show  $S_{21}$ . This plot can be formatted and configured using the various options in this section. The corresponding  $S_{21}$  and  $S_{11}$  data for the entire measurement is also saved automatically in a csv file once the measurement completes. The user can select between polar and rectangular cartesian plots. Furthermore, the user may add a grid, plot multiple measurement sweeps on the same plot, or view the plot in linear or dB scale with or without normalization. The user can also select the radial parameters of the polar plot as well as the independent variable. The display options section is shown in detail in Figure 3.12.

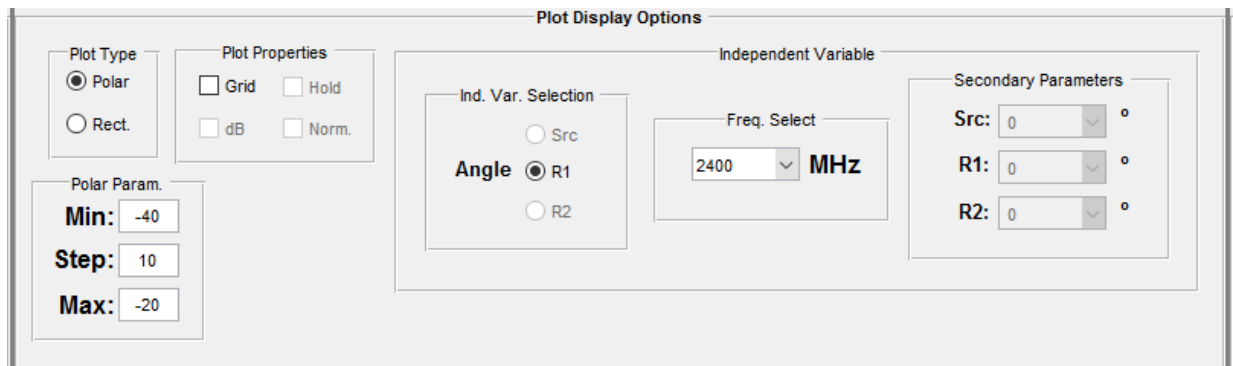


Figure 3.12 The ‘Plot Display Options’ section of the software interface.

### 3.2.5 System Messages

The user can receive guidance about the state and operation of the software from the system messages box. This box will direct the user in what they should do next to start a measurement as well as notify them of any errors that were encountered.

### 3.2.6 Plot Window

Once a measurement has started, a plot window will appear displaying the  $S_{21}$  data in real time with the format and plane-cut requested by the user in the plot display section. This window

is shown in Figure 3.14.

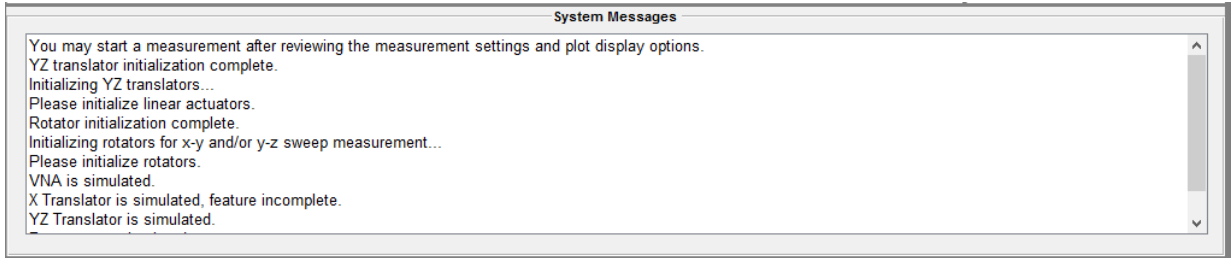


Figure 3.13 The ‘System Messages’ section of the software interface.

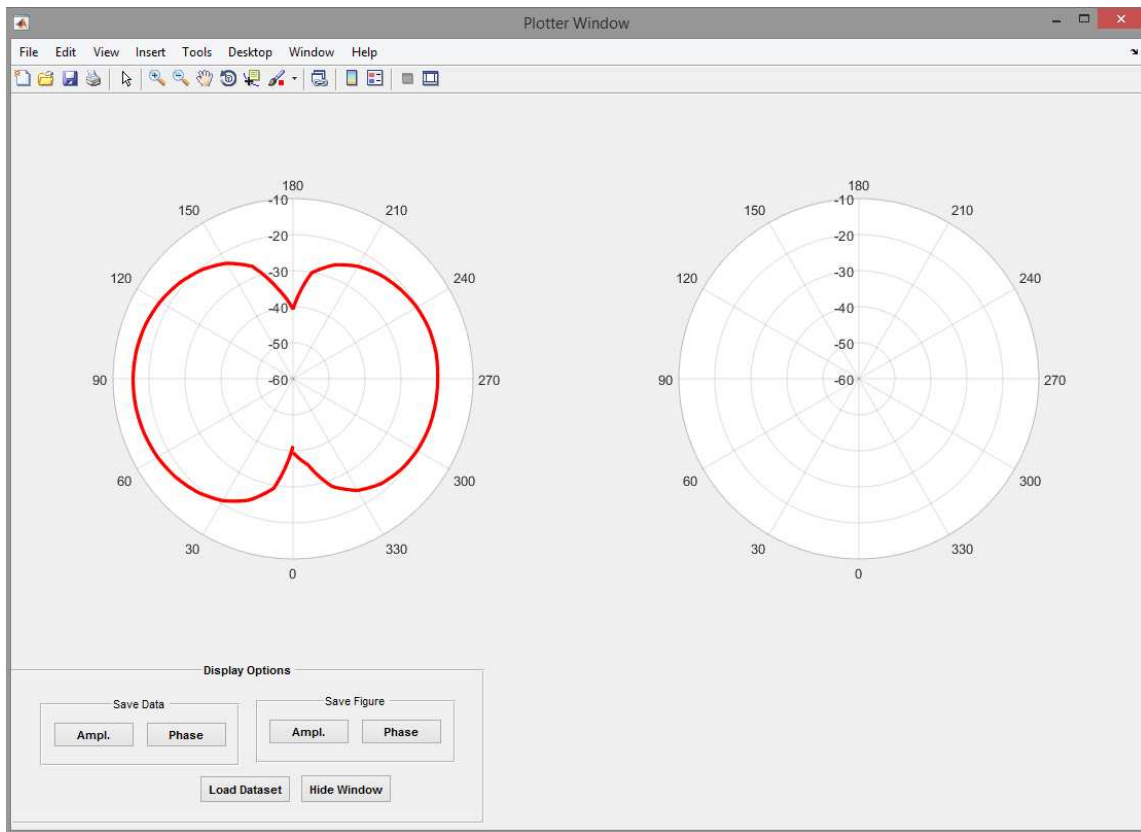


Figure 3.14 The plot window where  $S_{21}$  data is plotted during a measurement. The right plot is reserved for future simultaneous plotting capability. The ‘Display Options’ section is for future capabilities.

### 3.2.7 Saved Data Format

A truncated example of the data file output by the system during each measurement is shown in Figure 3.15. This csv file records the frequency and angular position of each rotary table

for every row of S-parameter data. The user can utilize different methods to easily parse this file in order to plot something of interest.

f(MHz)	SrcAngle(Deg)	R1Angle(Deg)	R2Angle(Deg)	S11(Re)	S11(Im)	S21(Re)	S21(Im)
2200.00	0	0	0	-6.22E-03	-5.08E-02	-1.40E-02	-4.33E-03
2202.00	0	0	0	-1.37E-02	-5.17E-02	-8.53E-03	1.49E-02
2204.00	0	0	0	-2.04E-02	-5.16E-02	1.42E-02	1.27E-02
2206.00	0	0	0	-2.63E-02	-5.12E-02	1.91E-02	-1.21E-02
2208.00	0	0	0	-3.53E-02	-4.75E-02	-7.25E-03	-2.29E-02
2210.00	0	0	0	-2.95E-02	-5.81E-02	-2.34E-02	1.64E-03

Figure 3.15 Truncated example of the data file automatically saved by the measurement system.

The system itself has a script that it utilizes to extract slices of data from these files that it can plot. This behavior is encapsulated in a method called ‘DataParser’, included in Appendix A. ‘DataParser’ requires the path to the data file, the frequency, and whether the user wants S<sub>21</sub> or S<sub>11</sub> data. The user must also provide any two angles to hold constant, leaving the last angle as the independent variable. For example, this could be the source and R2 rotator at an angle of five-degrees, leaving the R1 rotator as the independent variable. The method will then return the requested S-parameter’s real and imaginary data and the associated independent variable data.

An example usage of this method is:

```
s21Data = DataParser('Sim_Data\dipole_figure8.csv',2400,'r1',0,'src',0,'s21')
```

Which requests S<sub>21</sub> data as a function of the R2 rotator, at the frequency of 2.4 GHz and holding the R1 and source rotators at zero-degrees. The result of this method can then be converted into dB scale and then plotted:

```
s21dB = 20*log10(sqrt(s21Data(:,2).^2+s21Data(:,3).^2));
plot(s21Data(:,1),s21dB)
ylabel('|S21| (dB)')
```

```
xlabel('R2 Pos. (deg)')  
title('y-z plane cut of dipole')  
grid on
```

The result of this is shown in Figure 3.16. This data file was from a y-z plane-cut measurement of a dipole antenna. From Figure 3.16, it is evident that this is the expected data one should see from this data file.

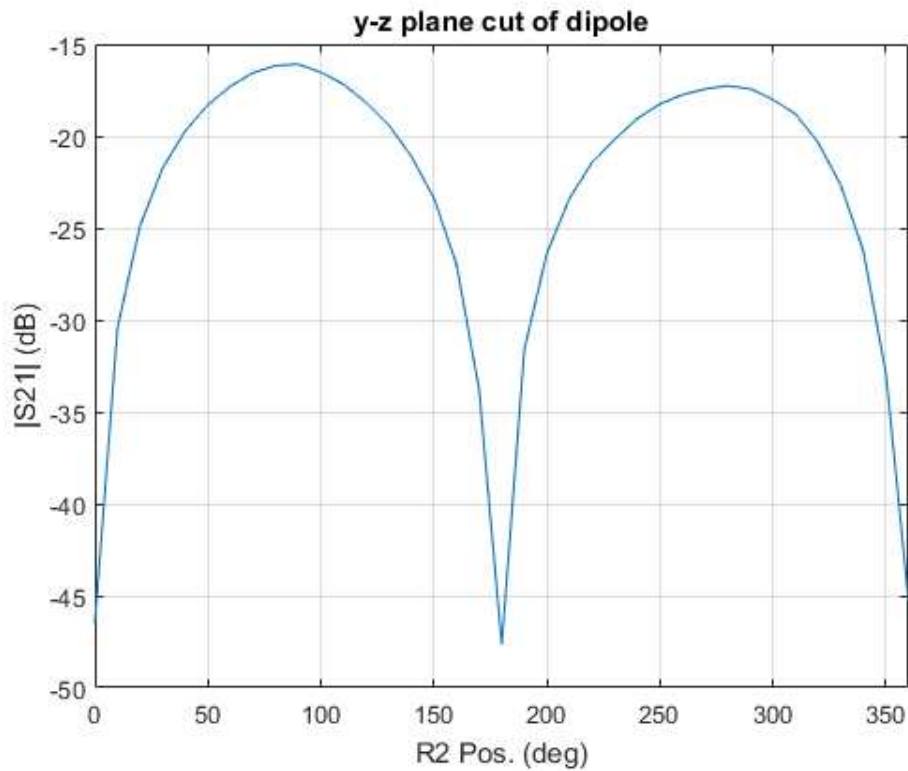


Figure 3.16 Rectangular plot of the data slice returned by the 'DataParser' method from a file containing data for a y-z plane-cut of a dipole.

## CHAPTER 4

### MEASUREMENT EXAMPLE

This chapter presents a walkthrough of utilizing the system to obtain the x-y and y-z plane-cuts of a dipole antenna. This example will utilize a 2.4 GHz dipole antenna and the E5080A VNA. First the antenna is mounted onto the AUT fixture, shown in Figure 4.1. Next, the user should follow the hardware startup procedure outlined in section 2.5. The user can compare the VNA connections to those shown in Figure 4.2. Now, the user can run the ‘Anechoic Init’ MATLAB code. The configuration used for this measurement is shown in Figure 4.3.

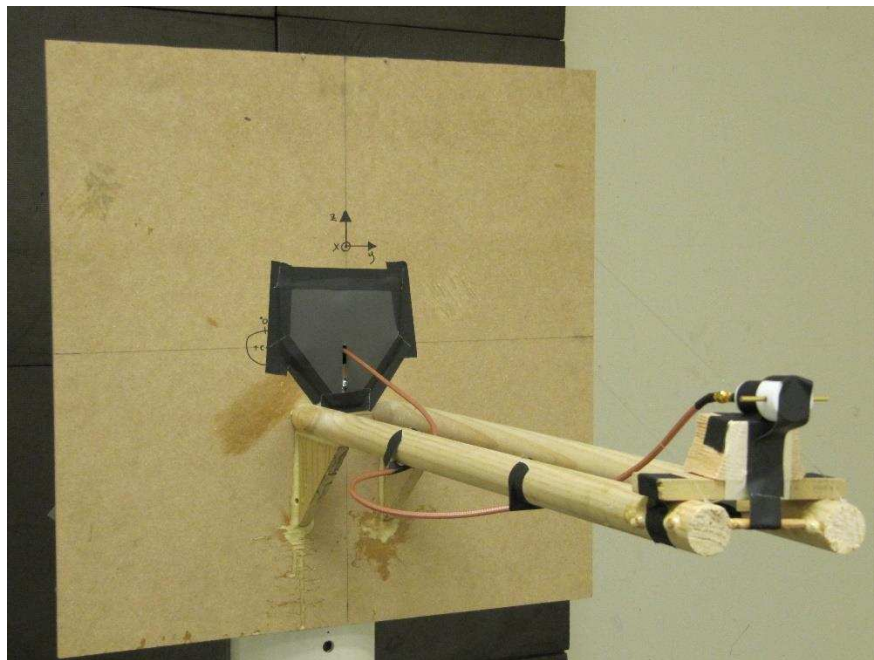


Figure 4.1 The 2.4 GHz dipole antenna mounted onto the AUT fixture.

After clicking ‘Done’, the main interface will open. The user will be directed to initialize the rotators and should then click the ‘Init Src + R1 + R2’ button in the ‘Rotator Setup’ section, shown in Figure 4.4. Once the rotators are done initializing, the user will then be directed to

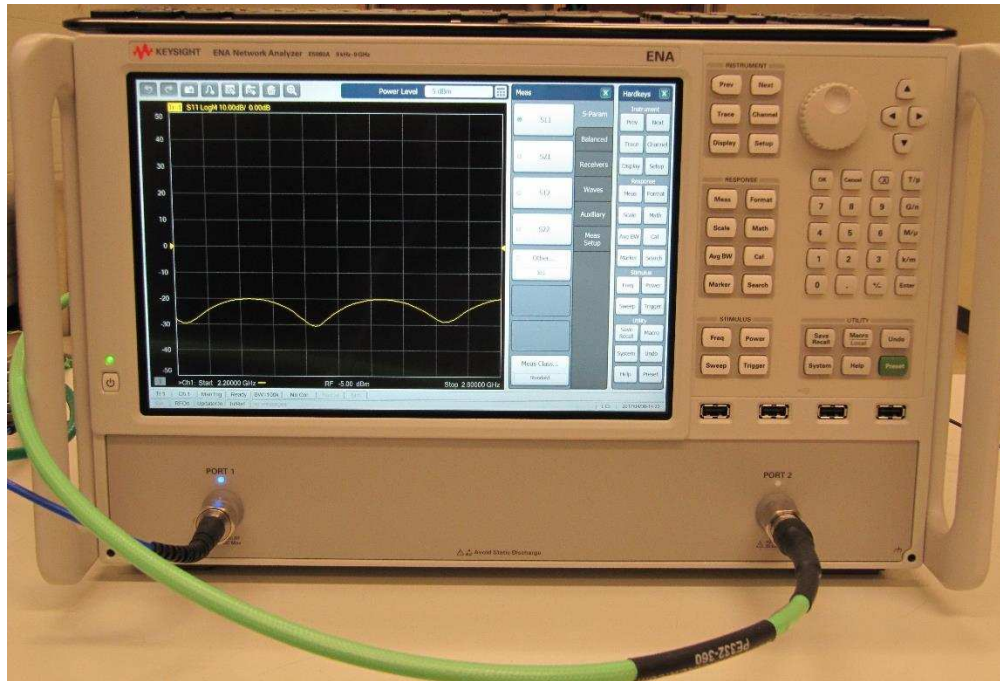


Figure 4.2 The E5080A VNA used for the measurement example. The blue cable connected to Port 1 connects to the input of the amplifier, while the green cable connected to Port 2 connects to the AUT.

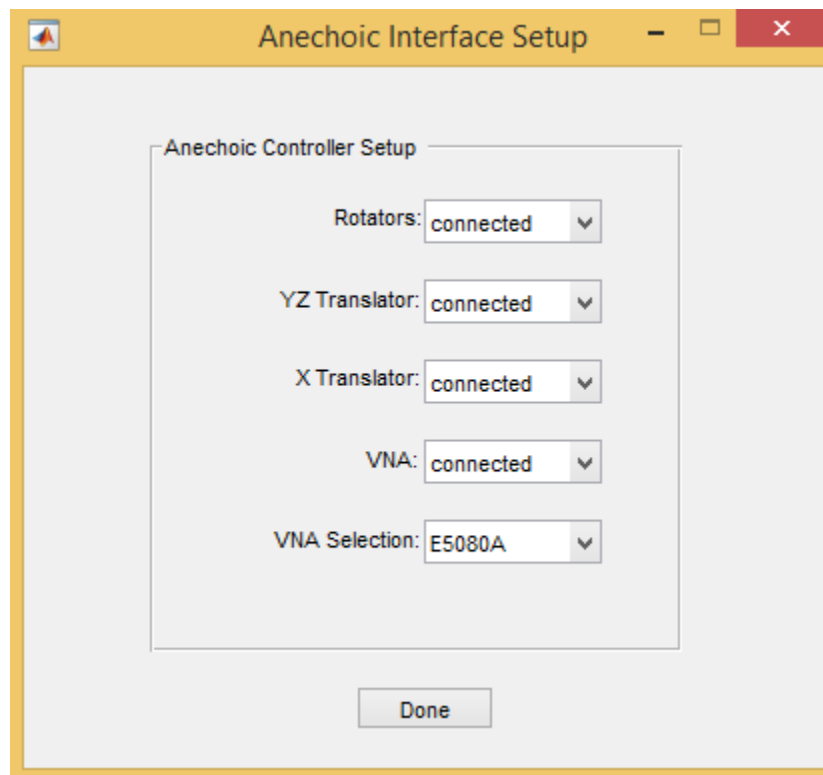


Figure 4.3 The startup configuration needed for the measurement example.

initialize the linear actuators. This can be done by clicking the ‘Initialize Linear Actuators’ button in the ‘Source Linear Actuator Control’ section, shown in Figure 4.5.

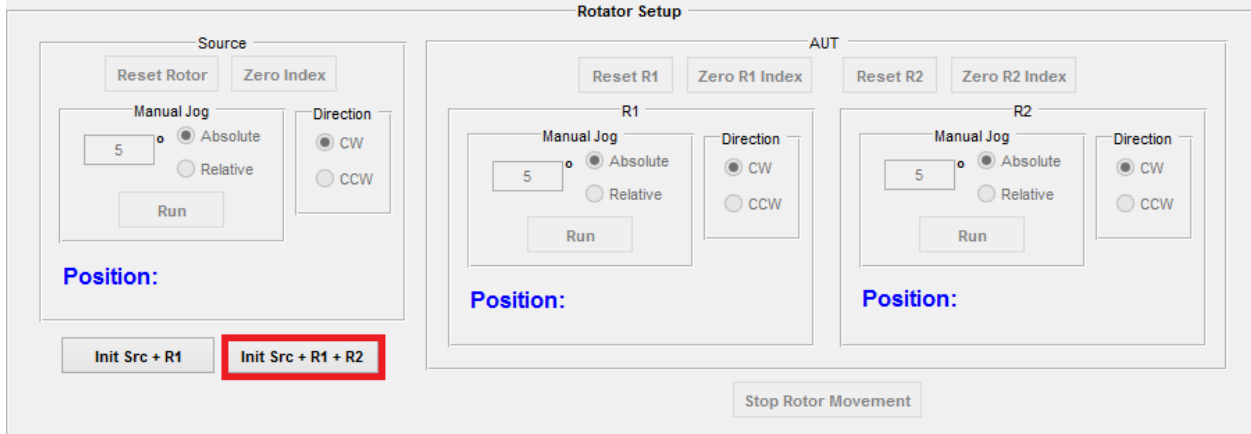


Figure 4.4 Initializing the rotators for the measurement example.

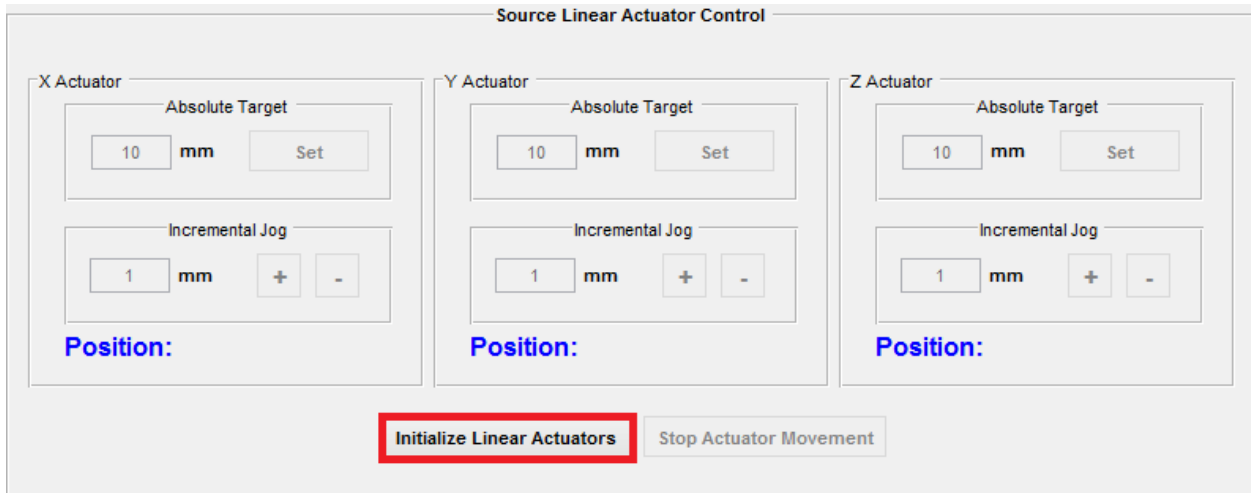


Figure 4.5 Initializing the linear actuators for the measurement example.

Once the actuators are initialized, the user must then align the source fixture with the dipole in the AUT fixture. For this antenna, this corresponds to maxing the position of both actuators. This can be done by moving the y actuator to 96 mm and the z actuator to 144 mm, which is shown in Figure 4.6. From Figure 4.6, it is apparent that the positions of the actuator do not match the requested values of 96 mm and 144 mm. This is because the position values shown are the

maximum allowed values for the actuators and these provided values of 96 mm and 144 mm serve to drive each actuator to the max. It is easier to input these whole numbers than the exact number shown on the screen. The source fixture before alignment and after alignment can be seen in Figure 4.7. Currently this process is manual but can be automated in the future using laser alignment.

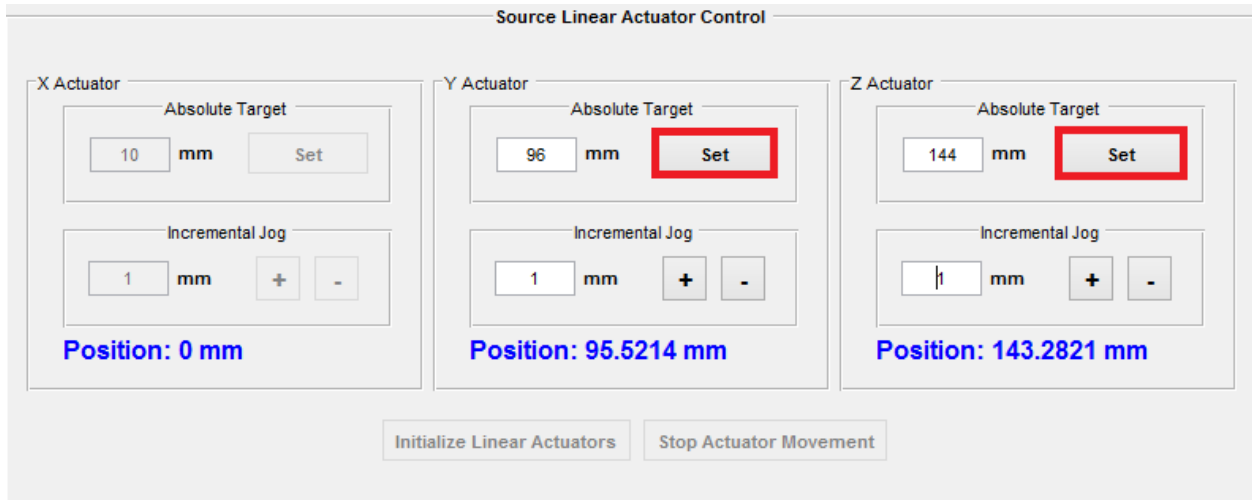


Figure 4.6 Aligning the source fixture to the AUT via the interface.

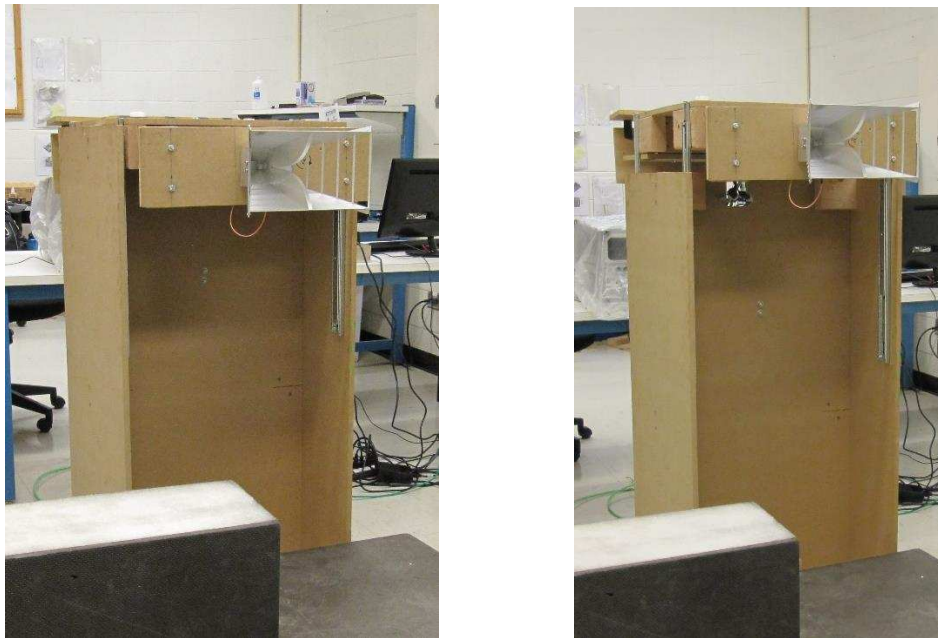


Figure 4.7 Source fixture before alignment (left) and source fixture after alignment (right).

Next, the user sets up the measurement parameters in the ‘Measurement Setup’ section, shown in Figure 4.8. To get the y-z plane-cut, or the figure-eight pattern, of this dipole, the user must select the ‘yz Sweep Plane’ option. To obtain the full cut, the sweep range must increment from zero to 360 degrees. For this example, the increment is ten-degrees. The frequency and power parameters in the ‘VNA Settings’ section default to those shown in Figure 4.8 and do not need to be adjusted for this antenna. Finally, the user should adjust the polar parameters in the ‘Plot Display Options’ section shown in Figure 4.9. This is to ensure the plot of the received signal is within range. The plot scale range can also be further adjusted after the measurement completes. Now, the user can then turn on the power supply for the amplifier and then start the measurement from the green ‘Start’ button.

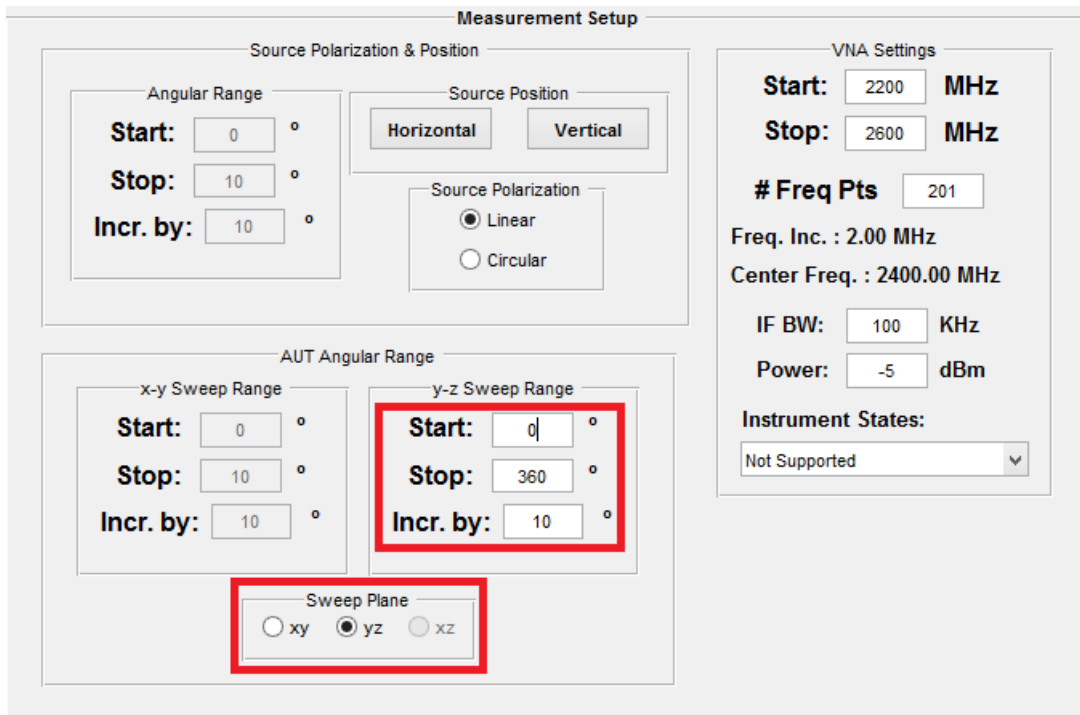


Figure 4.8 Setting up the measurement parameters for the y-z plane-cut of the measurement example.

The system will now perform the measurement. During the process, the rotary table R2 will move and the VNA will perform a frequency sweep at each angular position, returning the specified number of frequency points' worth of data. The data slice the user requested in the 'Plot Display Options' section will be plotted in real time at the specified frequency while the entire dataset is saved locally. Figure 4.10 and 4.11 show this process and Figure 4.12 shows the final expected data.

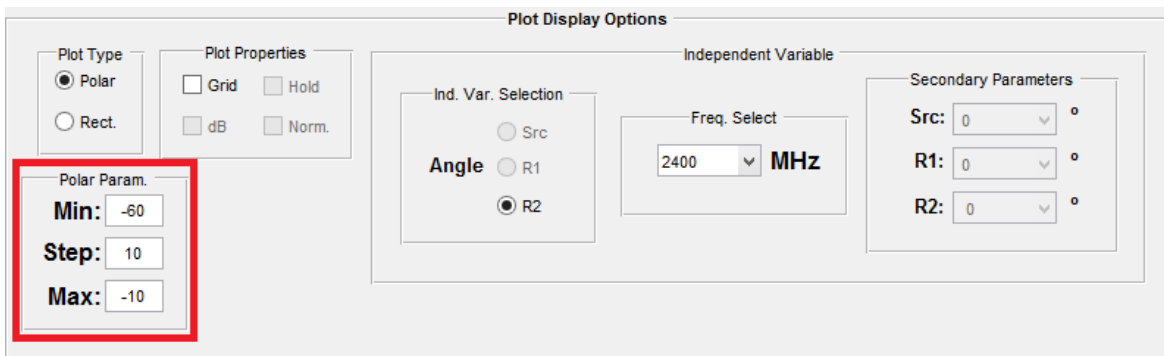


Figure 4.9 Adjusting the polar parameters for the measurement example.

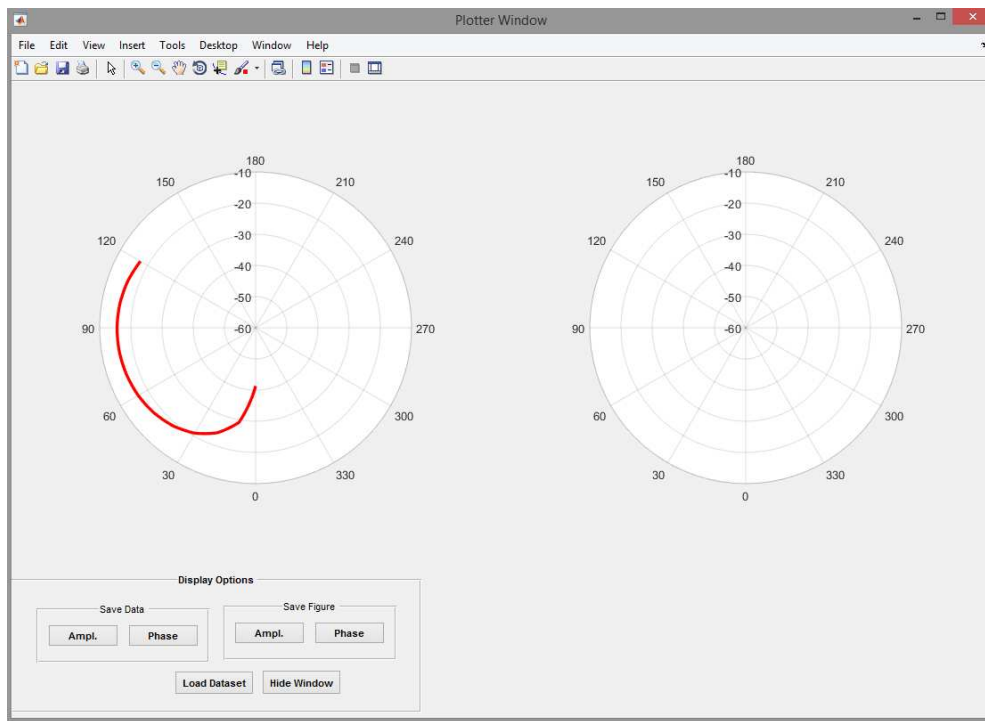


Figure 4.10 In-progress plotting of the y-z plane-cut data for the measurement example. The right plot is reserved for future simultaneous plotting capability. The 'Display Options' section is for future capabilities.

To get the other plane-cut, the user must offset the source antenna. This can be done multiple ways, the simplest is to press the 'Vertical' button in the 'Measurement Setup'. The user should also select the 'xy Plane Sweep' option and input a sweep from zero to 180 degrees. Both operations are shown in Figure 4.13. This moves the source horn antenna to the vertical position in Figure 4.14.



Figure 4.11 In-progress measurement of the y-z plane-cut for the measurement example.

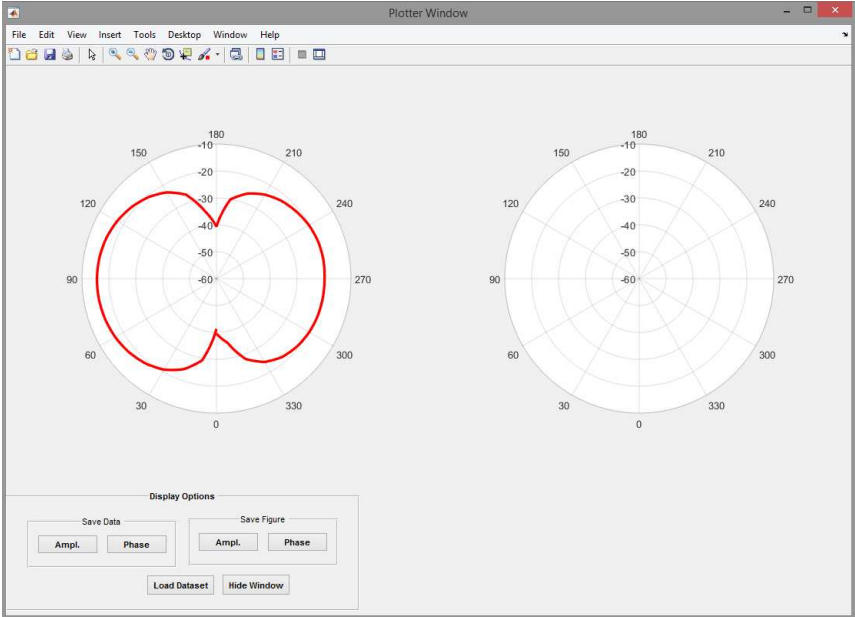


Figure 4.12 The final plot of the y-z plane-cut data for the measurement example.

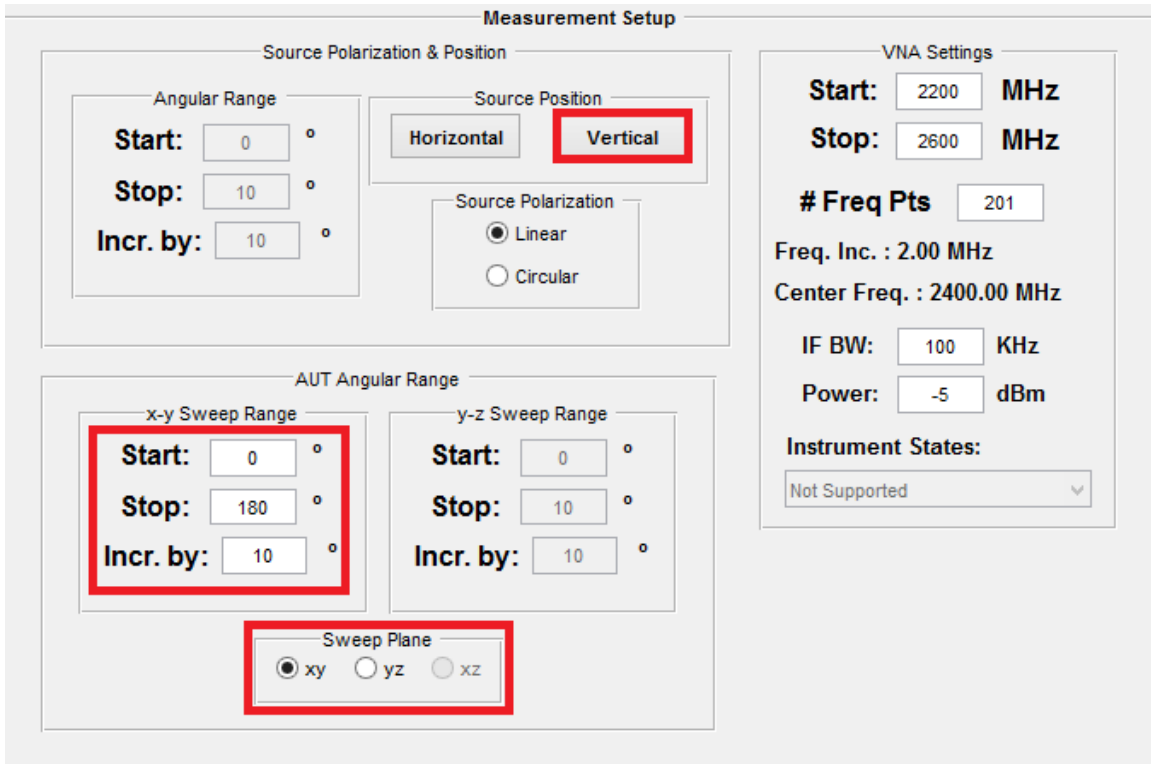


Figure 4.13 Setting up the measurement parameters for the x-y plane-cut of the measurement example.

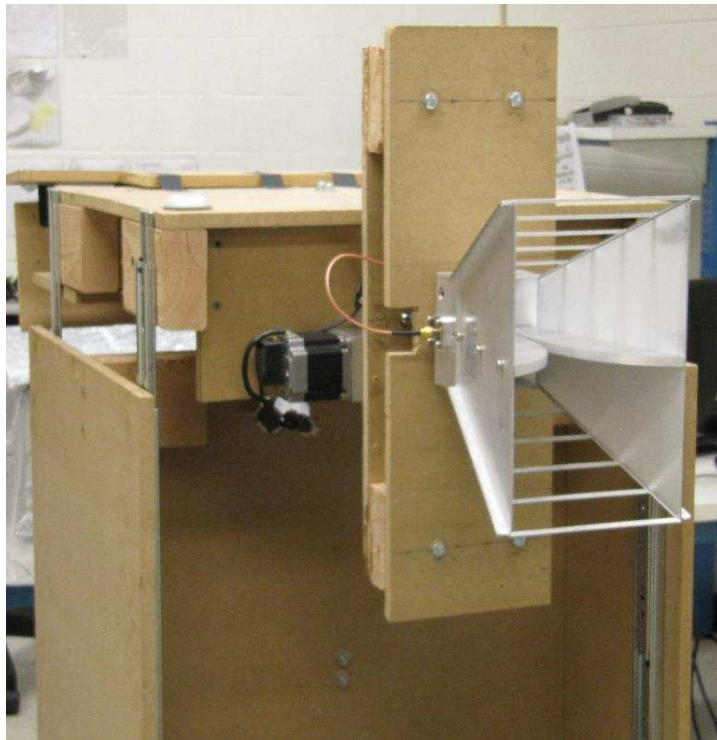


Figure 4.14 Source antenna moved to the vertical position for the x-y plane-cut of the measurement example.

Another offset must be applied to the R1 rotator so that the x-y plane sweep occurs over the expected angular positions. This can be done by utilizing the ‘Rotator Setup’ section and placing a value of ‘90’ in the ‘R1’ section. The ‘CCW’ option must be set so the rotator goes to the right. Once the rotator is done moving, the user should click the ‘Zero R1 Index’ button to set the zero-reference of the rotator. This ensures that the 90-degree position of the sweep points the AUT fixture towards the center of the source fixture as one would expect. This process is shown in Figure 4.15 and the result is shown in Figure 4.16. The user may now start the measurement by clicking the green ‘Start’ button. Like before, the system will plot data in real-time at each angular position. The progression of the measurement is shown in Figure 4.17 and Figure 4.18, with the final plot shown in Figure 4.19. One can see that the final plot is not quite perfectly a semi-circle as one would expect. This is attributed to the lack of absorbers on the walls of the anechoic chamber.

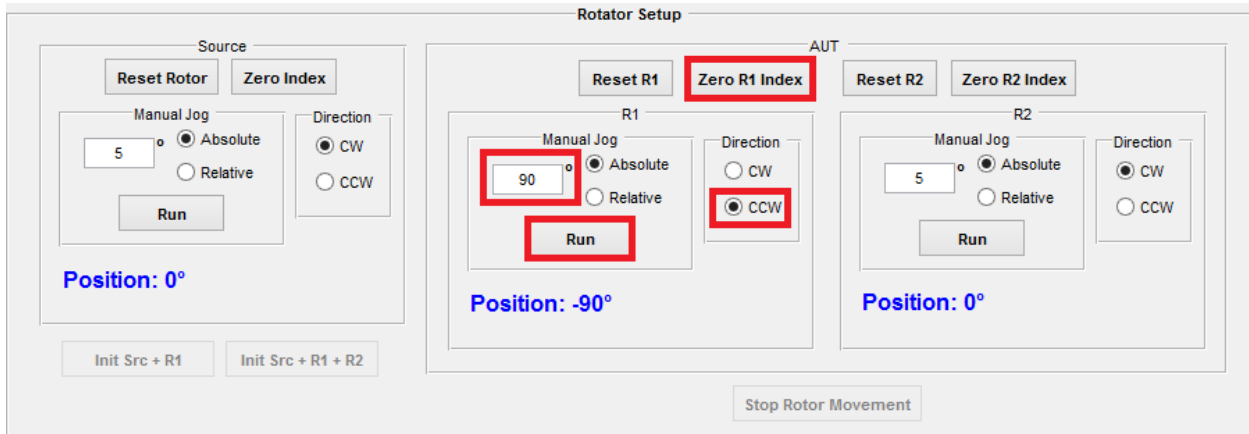


Figure 4.15 Offsetting the R1 rotator for the x-y plane-cut of the measurement example.

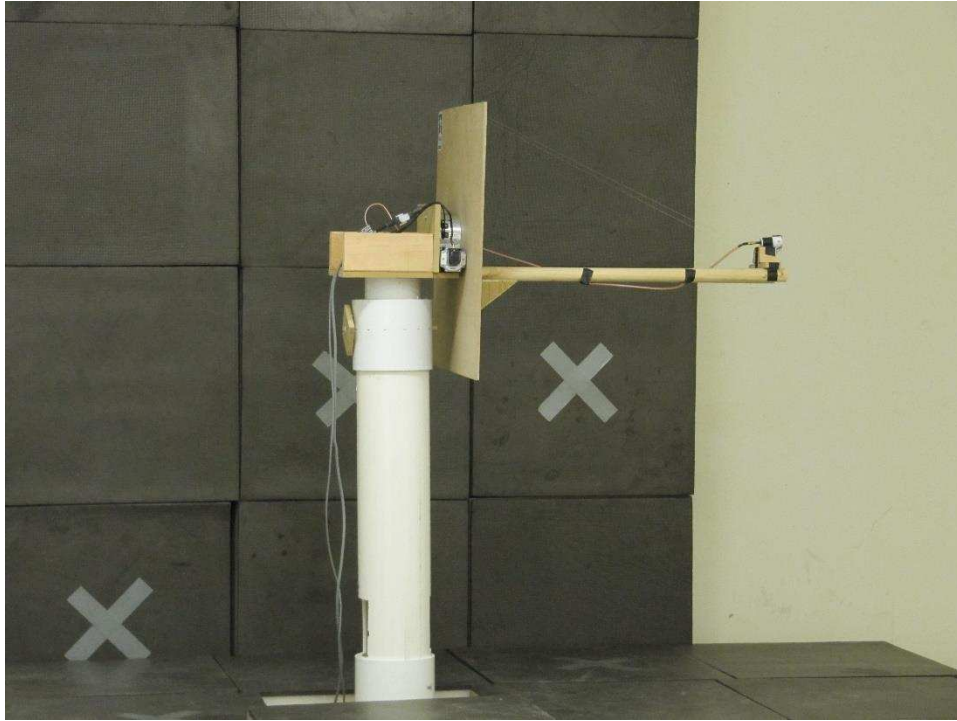


Figure 4.16 The R1 rotor offset for the x-y plane-cut of the measurement example.

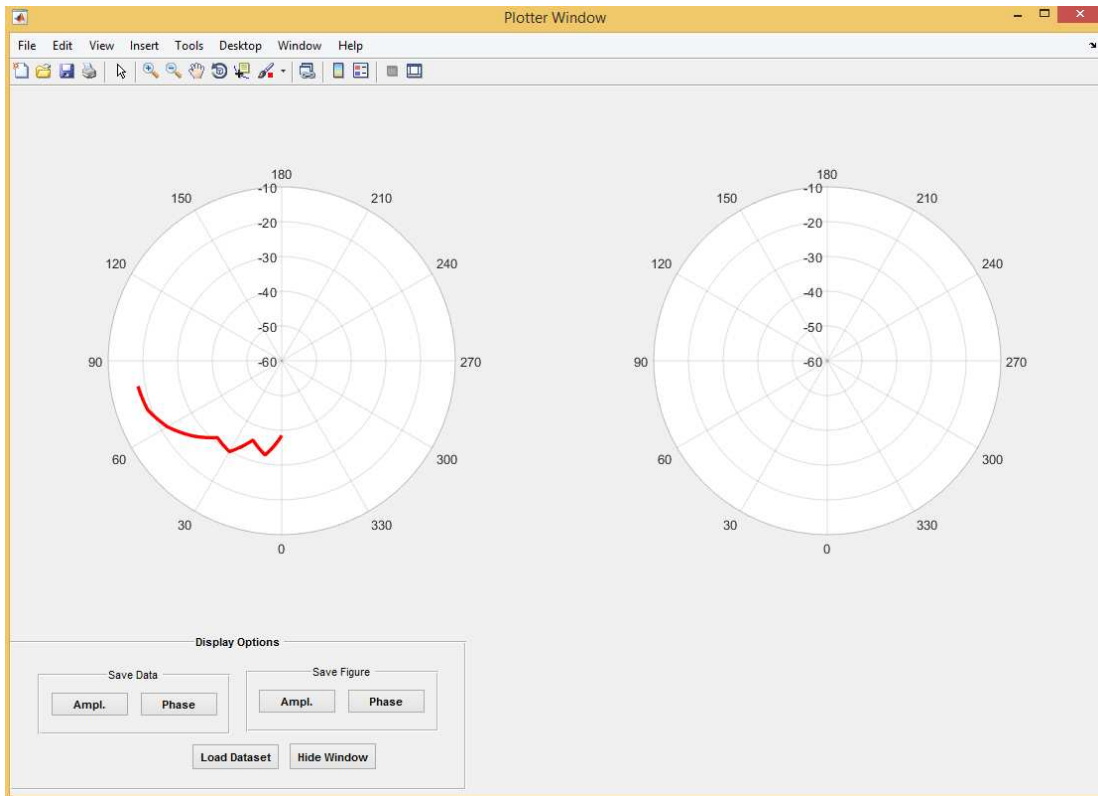


Figure 4.17 In-progress plotting of the x-y plane-cut data for the measurement example.



Figure 4.18 In-progress measurement of the x-y plane-cut for the measurement example.

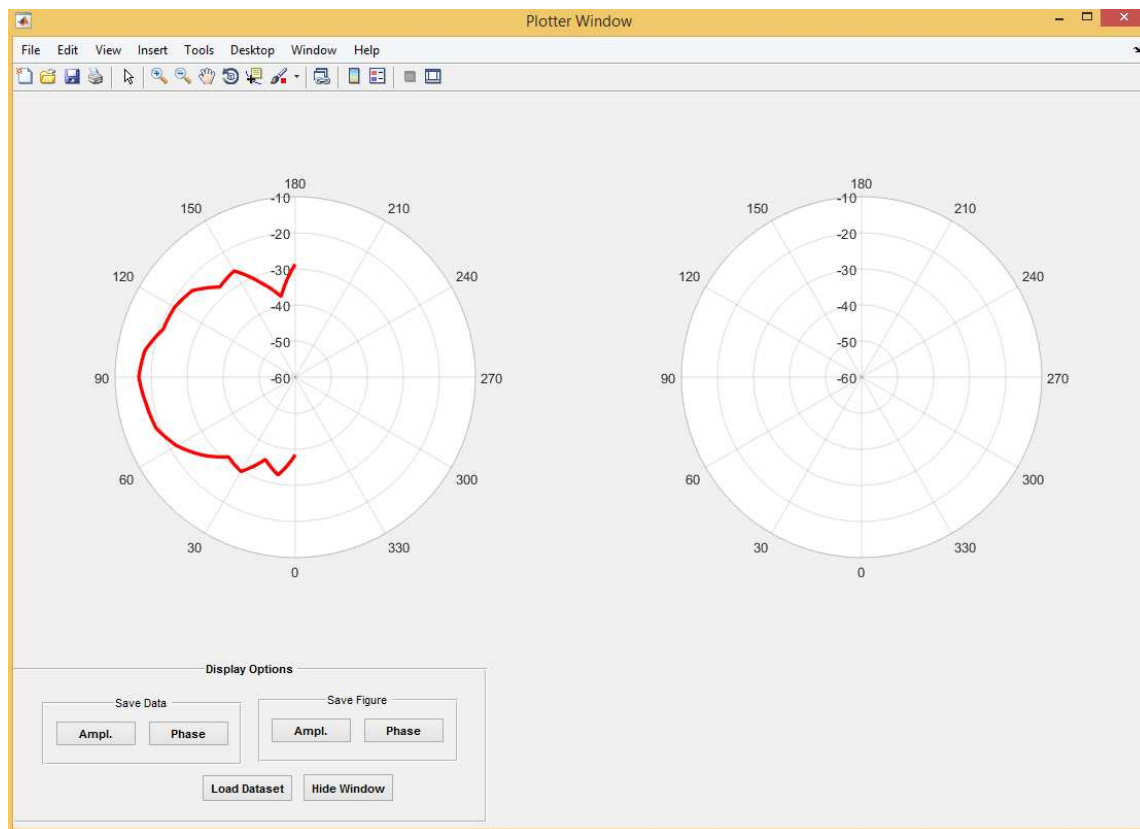


Figure 4.19 The final plot of the x-y plane-cut data for the measurement example.

## CHAPTER 5

### FUTURE UPGRADES AND CONCLUSION

The automated antenna measurement system presented here allows a user to determine the radiation pattern of an antenna under test. The user is presented with a guided procedure that guides the user through rotator setup, linear actuator setup, and measurement setup. Once the measurement parameters are defined, then the user can specify what is to be plotted and can view real-time results as the measurement progresses. This data is also simultaneously saved in a csv file for later post-processing.

This design brings several key improvements to the capability of automated antenna measurement systems. One key improvement is in the reusability and maintainability of the design. Because the different software code units are completely independent from one another, one can easily update the system for new hardware over time. Another key improvement is that the system has capability to work with a range of Keysight VNAs without having to change any underlying code. The VNA can be simply selected by the user at runtime. This brings many benefits such as being able to utilize different VNAs to cover different frequencies as well as allowing for continued chamber operation should one VNA need repair or factory recalibration. Furthermore, a lot of prototype antenna measurement system designs tend to overlook features such as safety limits and mechanisms that are intended to keep the system from breaking. This design provides a guided user experience that also has positioning limits built in that prevent the system from being run into a failure state. The combination of all these improvements creates a more robust and timeless automated antenna measurement system that can continue to be used for many years.

There were also many challenges in completing this system. One such challenge was the difficulty in preventing the user from running the rotary tables past certain positions. For

measurements that require both R1 and R2 on the AUT fixture, R1 must be limited between zero and 180 degrees, otherwise there is a risk that the fixture could collide with the rear wall of the chamber. Ideally, one could simply restrict the valid range of positions to these values, but this could not be done in this system. This is because the user can offset each rotary table to an arbitrary zero reference, which can shift the meaning of zero and 180. The solution for this problem was a rather complicated system of tracking the offsets.

Another challenge was defining the frame of reference that all the measurements angle parameters would take place against. Some meaning needs to be applied to the measurement sweep angles that would allow different users to have a consistent expectation of how the software should work. Ideally, one would choose either a  $\phi$  or  $\theta$  plane-cut measurement, as this correlates to what one would be looking to verify from analytic or simulation based results. However, in practice, this cannot be done globally since there are many possible antennas that could be measured with this system, each with different physical orientations needed to get a true  $\phi$  or  $\theta$  plane-cut measurement. Thus, it was decided to utilize the frame of reference of the fixtures for the different plane-cuts which provides the same meaning through any possible antenna selection since the rotary tables themselves do not move relative to the fixture they are mounted on.

However, there are many potential areas this work could be improved upon. One such example is the plotting functionality. While the current plotting functionality is adequate, it is very basic and could be upgraded to display patterns for multiple frequencies simultaneously. Furthermore, more work needs to be done to format the plots so the user knows what is being plotted without having to refer to the main interface window. Another area of improvement is in the user interface. Currently, provisions were made for basic input sanitization, but more work needs to be done to check if the values provided make sense and describe to the user what the

acceptable range of values are for a parameter using tooltips. Additional algorithms can be added to allow for circularly polarized measurements as well as allowing for a gain measurement process. The alignment process could also be improved by integrating a laser pointing mechanism.

## REFERENCES

- [1] R. C. Johnson, *Antenna Engineering Handbook*, New York: McGraw-Hill, Inc., 1993.
- [2] C. A. Balanis, *Antenna Theory Analysis and Design*, New York: John Wiley & Sons, Inc., 1997.
- [3] J. S. Hollis, T. J. Lyon, and L. Clayton, Jr., *Microwave Antenna Measurements*, Atlanta, GA: Scientific-Atlanta, Inc., 1970.
- [4] S. Gregson, J. McCormick, and C. Parini, *Principles of Planar Near-field Antenna Measurements*, UK: IET, 2007.
- [5] W. H. Kummer and E. S. Gillespie, "Antenna Measurements," *Proc. of the IEEE*, vol. 66, no. 4, pp. 483-507, Apr., 1978.
- [6] S. S. Osofsky and S. E. Schwarz, "Design and Performance of a Non-Contacting Probe for Measurements on High-Frequency Planar Circuits," *IEEE Trans. Microw. Theory Tech.*, vol. 40, no. 8, pp. 1701-1708, Aug. 1992.
- [7] A. D. Yaghjian, "An Overview of Near-Field Antenna Measurements," *IEEE Trans. Antennas Prop.*, vol. 34, no. 1, pp. 30-45, Jan. 1986.
- [8] R. C. Johnson, H. A. Ecker, and J. S. Hollis, "Determination of Far-Field Antenna Patterns from Near-Field Measurements," *Proc. of the IEEE*, vol. 61, no. 12, pp. 1668-1693, Dec. 1973.
- [9] D. Paris, W. M. Leach Jr., and E. B. Joy, "Basic Theory of Probe-Compensated Near-Field Measurements," *IEEE Trans. Antennas Prop.*, vol. 26, no. 3, pp. 373-379, May 1978.
- [10] P. Petre and T. K. Sarkar, "A planar near-field to far-field transformation using an equivalent magnetic current approach," in *Antennas and Propagation Society International Symposium*, Chicago, IL, pp. 1534-1537, 1992.
- [11] T. K. Sarkar and A. Taaghoul, "Near-field to near/far-field transformation for arbitrary near-field geometry utilizing an equivalent electric current and MoM," *IEEE Antennas Prop. Mag.*, vol. 47, no. 3, pp. 566-573, Aug. 1996.
- [12] *IEEE Standard Test Procedures for Antennas*, IEEE Std 149-1979, 1979.
- [13] K. Haner and G. Masters, "State-of-the-art Near-field Measurement System," in *Antenna Measurement Techniques Association Conference*, 1995.
- [14] C. Garner, "Anechoic Chamber Instrumentation Control and Data Collection," B.S. Honors Thesis, Dept. Elect. Eng., Univ. of Mississippi, Oxford, MS, 2013.

- [15] A. M. Choong, "An Anechoic Chamber System for Antenna Pattern Measurements," M.S. Thesis, Dept. Elect. Eng., Univ. of Mississippi, Oxford, MS, 2006.
- [16] Velmex, Inc. <http://www.velmex.com/index.html>
- [17] Pololu Robotics & Electronics. <https://www.pololu.com/>

## APPENDIX A

### DATA PARSER CODE

```
function result =
DataParser(fileName,f,param1Name,param1Val,param2Name,param2Val,dataType)
if ~strcmpi(param1Name,'Src') && ~strcmpi(param1Name,'R1') &&
~strcmpi(param1Name,'R2')
    error('Param 1 is not valid; must be either Src, R1, or R2');
end
if ~strcmpi(param2Name,'Src') && ~strcmpi(param2Name,'R1') &&
~strcmpi(param2Name,'R2')
    error('Param 2 is not valid; must be either Src, R1, or R2');
end
if strcmpi(param1Name,param2Name)
    error('Param 1 and Param 2 cannot be the same');
end
if ~strcmpi(dataType,'S11') && ~strcmpi(dataType,'S21')
    error('Data Type must be either S11 or S21');
end

if strcmpi(dataType,'S11')
    dataPos = 5;
else
    dataPos = 7;
end

if strcmpi(param1Name,'Src')
    if strcmpi(param2Name,'R1')
        pSPos = 4;
    elseif strcmpi(param2Name,'R2')
        pSPos = 3;
    end
elseif strcmpi(param1Name,'R1')
    if strcmpi(param2Name,'Src')
        pSPos = 4;
    elseif strcmpi(param2Name,'R2')
        pSPos = 2;
    end
else
    if strcmpi(param2Name,'Src')
        pSPos = 3;
    elseif strcmpi(param2Name,'R1')
        pSPos = 2;
    end
end
end
```

```

if strcmpi(param1Name,'Src')
    p1Pos = 2;
elseif strcmpi(param1Name,'R1')
    p1Pos = 3;
else
    p1Pos = 4;
end

if strcmpi(param2Name,'Src')
    p2Pos = 2;
elseif strcmpi(param2Name,'R1')
    p2Pos = 3;
else
    p2Pos = 4;
end

fullData = csvread(fileName,1,0);

result = [];
numRows = size(fullData,1);
for i = 1:numRows
    row = fullData(i,:);
    if row(1) == f
        if row(p1Pos) == param1Val
            if row(p2Pos) == param2Val
                result = [result;[row(pSPos) row(dataPos) row(dataPos+1)]];
            end
        end
    end
end
end
end

```